



**HAL**  
open science

## **TMPRSS2 is a functional receptor for human coronavirus HKU1**

Nell Saunders, Ignacio Fernandez, Cyril Planchais, Vincent Michel, Maaran Michael Rajah, Eduard Baquero Salazar, Jeanne Postal, Françoise Porrot, Florence Guivel-Benhassine, Catherine Blanc, et al.

► **To cite this version:**

Nell Saunders, Ignacio Fernandez, Cyril Planchais, Vincent Michel, Maaran Michael Rajah, et al..  
TMPRSS2 is a functional receptor for human coronavirus HKU1. *Nature*, 2023, 624 (7990), pp.207-214. 10.1038/s41586-023-06761-7 . hal-04372694

**HAL Id: hal-04372694**

**<https://hal.science/hal-04372694>**

Submitted on 27 Mar 2024

**HAL** is a multi-disciplinary open access archive for the deposit and dissemination of scientific research documents, whether they are published or not. The documents may come from teaching and research institutions in France or abroad, or from public or private research centers.

L'archive ouverte pluridisciplinaire **HAL**, est destinée au dépôt et à la diffusion de documents scientifiques de niveau recherche, publiés ou non, émanant des établissements d'enseignement et de recherche français ou étrangers, des laboratoires publics ou privés.

1 **TMPRSS2 is a functional receptor for human coronavirus HKU1**

2

3 Nell Saunders<sup>1</sup>, Ignacio Fernandez<sup>2</sup>, Cyril Planchais<sup>3</sup>, Vincent Michel<sup>4</sup>, Maaran Michael  
4 Rajah<sup>1</sup>, Eduard Baquero Salazar<sup>5</sup>, Jeanne Postal<sup>1</sup>, Francoise Porrot<sup>1</sup>, Florence Guivel-  
5 Benhassine<sup>1</sup>, Catherine Blanc<sup>6</sup>, Gaëlle Chauveau-Le Fric<sup>7</sup>, Augustin Martin<sup>1</sup>, Ludivine  
6 Grzelak<sup>1</sup>, Rischa Maya Oktavia<sup>2</sup>, Annalisa Meola<sup>2</sup>, Olivia Ahouzi<sup>2</sup>, Hunter Hoover-Watson<sup>1</sup>,  
7 Matthieu Prot<sup>8</sup>, Deborah Delaune<sup>8,13</sup>, Marion Cornelissen<sup>9,10</sup>, Martin Deijs<sup>10,11</sup>, Véronique  
8 Meriaux<sup>7</sup>, Hugo Mouquet<sup>3</sup>, Etienne Simon-Lorière<sup>8,14</sup>, Lia van der Hoek<sup>10,11</sup>, Pierre Lafaye<sup>7</sup>,  
9 Felix Rey<sup>2</sup>, Julian Buchrieser<sup>1,#,\*</sup> and Olivier Schwartz<sup>1,12,#,\*</sup>

10

11 <sup>1</sup>Virus & Immunity Unit, Institut Pasteur, Université de Paris Cité, CNRS UMR 3569, Paris, France

12 <sup>2</sup>Structural Virology Unit, Institut Pasteur, Université de Paris Cité, CNRS UMR 3569, Paris, France

13 <sup>3</sup>Humoral Immunology Unit, Institut Pasteur, Université de Paris Cité, INSERM U1222, Paris, France

14 <sup>4</sup>Pathogenesis of Vascular Infections Unit, Institut Pasteur, INSERM, Paris, France.

15 <sup>5</sup>Nanoimaging core, Institut Pasteur, Université de Paris Cité, INSERM U1222, Paris, France

16 <sup>6</sup>Pasteur-TheraVectys Joint Lab, Institut Pasteur, Université de Paris Cité, Paris, France

17 <sup>7</sup>Antibody Engineering Platform, C2RT, Institut Pasteur, Université de Paris Cité, CNRS UMR 3528,  
18 Paris, France.

19 <sup>8</sup>G5 Evolutionary Genomics of RNA Viruses, Institut Pasteur, Paris, France.

20 <sup>9</sup>Department of Medical Microbiology and Infection Prevention, Amsterdam UMC, Molecular  
21 Diagnostic Unit, University of Amsterdam, 1105 AZ Amsterdam, Netherlands.

22 <sup>10</sup>Amsterdam Institute for Infection and Immunity, Amsterdam, The Netherlands

23 <sup>11</sup>Department of Medical Microbiology and Infection Prevention, Amsterdam UMC, Laboratory of  
24 Experimental Virology, University of Amsterdam, 1105 AZ Amsterdam, Netherlands.

25 <sup>12</sup>Vaccine Research Institute, Creteil, France

26 <sup>13</sup>Institut de Recherche Biomédicale des Armées, Brétigny-sur-Orge, France

27 <sup>14</sup>National Reference Center for viruses of respiratory infections, Institut Pasteur, Paris, France.

28 #Co-last authors

29 \*Corresponding authors

30

31 **Abstract**

32

33 Four endemic seasonal human coronaviruses causing common colds, HKU1, 229E, NL63  
34 and OC43 circulate worldwide<sup>1</sup>. After binding to cellular receptors, coronavirus spike proteins  
35 are primed for fusion by transmembrane-serine protease 2 (TMPRSS2) or endosomal  
36 cathepsins<sup>2-9</sup>. NL63 uses angiotensin-converting enzyme 2 (ACE2) as a receptor<sup>10</sup>, whereas  
37 229E uses human aminopeptidase-N<sup>11</sup>. HKU1 and OC43 spikes bind cells through 9-O-  
38 acetylated sialic acid but their protein receptors remain unknown<sup>12</sup>. Here, we show that  
39 TMPRSS2 is a functional receptor for HKU1. TMPRSS2 triggers HKU1 spike-mediated cell-  
40 cell fusion and pseudovirus infection. Catalytically inactive TMPRSS2 mutants do not cleave  
41 HKU1 spike but allow pseudovirus infection. Furthermore, TMPRSS2 binds with high affinity  
42 to the HKU1 receptor binding domain (RBD) ( $K_d$  334 and 137 nM for HKU1A and HKU1B  
43 genotypes) but not to SARS-CoV-2. Conserved amino acids within HKU1 RBD are essential  
44 for binding to TMPRSS2 and pseudovirus infection. Newly designed anti-TMPRSS2  
45 nanobodies potently inhibit HKU1 spike attachment to TMPRSS2, fusion and pseudovirus  
46 infection. The nanobodies also reduce infection of primary human bronchial cells by an  
47 authentic HKU-1 virus. Our findings illustrate the various evolution strategies of coronaviruses,  
48 which use TMPRSS2 to either directly bind to target cells or to prime their spike for membrane  
49 fusion and entry.

50

51

52 **Main**

53 HKU1 was first identified from an elderly patient with severe pneumonia in Hong Kong in  
54 2005<sup>13</sup>. HKU1 was later shown to cause common cold and benign respiratory symptoms, but  
55 complications include severe lower respiratory infections, particularly in young children, the  
56 elderly and immunocompromised individuals<sup>14</sup>. It is estimated that 70% of children seroconvert  
57 before the age of 6<sup>15</sup>. The global seroprevalence of HKU1 is similar to other seasonal human  
58 coronaviruses (hCoV) and is between 75 and 95%<sup>15-17</sup>. Three main viral genotypes have been  
59 identified, HKU1A, B and C. HKU1A and B spikes have 85% identity (Fig. 1a). HKU1C is a  
60 HKU1A/B recombinant and its spike shares 99% identity with HKU1B. Conserved regions in  
61 the HKU1A and B spikes include a putative RBD with a Receptor Binding Motif (RBM)<sup>18,19</sup>,  
62 S1/S2 and S2/S2' cleavage sites<sup>20</sup> (Fig.1a).

63 Both HKU1 and OC43 spikes bind to 9-O-acetylated  $\alpha$ 2,8 linked disialosides on target  
64 cells<sup>12,21,22</sup>. Their protein receptors have not been identified. After receptor binding, the

65 coronavirus spike is cleaved at the S2' site by membrane bound proteases, such as TMPRSS2,  
66 or by endosomal cathepsins, resulting in a conformational change of S2 that projects the fusion  
67 peptide into the target membrane to drive fusion<sup>23</sup>. TMPRSS2 belongs to the type II  
68 transmembrane serine protease (TTSP) family that comprises 19 cell-surface enzymes<sup>24,25</sup>.  
69 TTSPs are involved in many processes, including epithelial homeostasis, extracellular matrix  
70 degradation, hormone and growth factor activation, and initiation of proteolytic cascades  
71 through cleavage of membrane cellular proteins<sup>24</sup>. TMPRSS2 primes coronavirus spikes and  
72 other viral envelope glycoproteins, such as influenza hemagglutinin, enabling fusion<sup>26</sup>. TTSPs  
73 are synthesized as single-chain proenzymes that require proteolytic activation<sup>24</sup>. TMPRSS2  
74 undergoes autocleavage into two subunits that remain attached by a disulfide bond<sup>27</sup>. In the  
75 respiratory tract, TMPRSS2 is expressed in nasal, bronchial and small airways tissues, and more  
76 particularly in ciliated cells that are the main target of HKU1<sup>28,29</sup>. Here, using cell-cell fusion  
77 assays, infections with pseudovirus and live virus, as well as *in vitro* binding tests, we identify  
78 TMPRSS2 as a high-affinity receptor for HKU1.

79

#### 80 **Generation of anti-TMPRSS2 nanobodies**

81 To our knowledge, there are no currently available anti-TMPRSS2 antibodies that allow cell  
82 surface staining, as most of the existing ones are directed towards cytosolic fragments of the  
83 protein. We thus immunized an alpaca with the soluble ectodomain of a catalytically inactive  
84 TMPRSS2 (S441A mutant) to produce VHH single-chain nanobodies. We isolated 5 VHHs  
85 (A01, F05, A07, C11 and D01) that bind with an affinity in the nanomolar range to soluble  
86 S441A TMPRSS2 (Extended Data Fig. 1a, Extended Data Table 1). We selected one VHH with  
87 the highest affinity (A01) in order to generate a dimeric antibody with a human Fc domain that  
88 efficiently stained TMPRSS2+ cells (Extended Data Fig. 1b).

89

#### 90 **TMPRSS2 triggers spike-dependent fusion**

91 To investigate the effect of TMPRSS2 on HKU1 spike mediated fusion, we generated  
92 plasmids encoding for the HKU1A (isolate N1 - NCBI: txid443239) and B (Isolate N5 - NCBI:  
93 txid443241) spikes (Fig. 1a). In 293T cells that do not express TMPRSS2, transient transfection  
94 led to surface expression of the two proteins, as assessed by flow cytometry using mAb10, a  
95 pan S2 coronavirus antibody<sup>30</sup> (Extended Data Fig. 2a). To study cell-cell fusion, we used a  
96 GFP-Split based model in which fused cells become GFP+ (Fig. 1b)<sup>31</sup>. HKU1A and B spikes  
97 did not induce fusion alone but were highly fusogenic when co-expressed with TMPRSS2 in  
98 293T cells (Fig. 1b, Extended Data Fig. 2b). In contrast, in experiments run in parallel, the

99 SARS-CoV-2 spike induced fusion when co-expressed with ACE2 and not with TMPRSS2  
100 (Extended Data Fig. 2c). HKU1 also triggered syncytia when co-expressed with TMPRSS2 in  
101 U2OS cells (Extended Data Fig. 2d).

102 As a control of specificity for HKU1 fusion, we tested a panel of 12 other surface proteases,  
103 including the coronavirus receptors aminopeptidase-N (APN), dipeptidyl peptidase-4 (DPP4)  
104 and ACE2, as well as TMPRSS4 and TMPRSS11D, that have been reported to cleave the  
105 SARS-CoV-2 spikes<sup>32-34</sup>. The proteases were correctly expressed, as assessed by flow  
106 cytometry (Extended Data Fig. 2e-i), but only TMPRSS2 triggered cell-cell fusion (Fig. 1c).

107 We next generated fluorescent TMPRSS2-mNeonGreen and HKU1A Spike-mScarlet-I to  
108 follow fusion by video microscopy. When mixed 24 h after transfection, cells expressing spike  
109 and cells expressing TMPRSS2 formed syncytia in less than 1 h, indicating that this process is  
110 rapid (Extended Data Fig. 2j, Supp. videos 1-2). By expressing TMPRSS2 either on donor cells  
111 (spike-transfected) or acceptor cells, we observed that the protease had to be on acceptor cells,  
112 opposite of the spike to induce high levels of fusion (Fig. 1d).

113 We then investigated whether endogenous levels of TMPRSS2 were sufficient to induce  
114 HKU1 spike-dependent fusion. We mixed HKU1A spike-expressing 293T donor cells with  
115 Caco2 acceptor cells, that endogenously express low levels of TMRPSS2<sup>35</sup> (Extended Data Fig.  
116 3). Spike expressing cells fused with parental Caco2 cells but not with Caco2 TMPRSS2-KO  
117 cells, a Caco2 derivative in which the *tmprss2* gene was knocked down by CRISPR-Cas9 (Fig.  
118 1e, Extended Data Fig. 3a-c). Silencing of TMPRSS2 using siRNA in Caco2 cells also  
119 significantly reduced fusion with spike-expressing 293T cells (Extended Data Fig. 3d).

120 Altogether, these results indicate that TMPRSS2 expression enables HKU1A and B spike-  
121 mediated cell-cell fusion.

122

### 123 **Inactive TMPRSS2 allows HKU1 infection**

124 To further analyze the role of TMPRSS2 in HKU1 spike fusion, we generated two well-  
125 characterized TMPRSS2 mutants, R255Q and S441A<sup>27</sup> (Fig. 2a). R255 is in the auto-cleavage  
126 site, and S441 is in the catalytic site; both mutations prevent TMPRSS2 autocleavage and  
127 activity. As expected, R255Q and S441A were correctly expressed in 293T cells but lacked  
128 catalytic activity, measured with a substrate generating a fluorescent signal upon cleavage<sup>36</sup>  
129 (Extended Data Fig. 4a). We then studied the cleavage profile of TMPRSS2 and HKU1 spike  
130 by western blot (Fig. 2b). We focused our analysis on HKU1A spike since none of the  
131 polyclonal or monoclonal antibodies tested recognized the HKU1B spike by western blot.  
132 When expressed alone, WT TMPRSS2 was cleaved while the mutants were not. When the

133 HKU1 spike was present, a similar profile of TMPRSS2 processing was observed. Without  
134 TMPRSS2, the spike was partially cleaved into S1 and S2 subunits (Fig. 2b), most likely at the  
135 polybasic furin cleavage S1/S2 site (Fig. 1a). WT TMPRSS2, but not the catalytically inactive  
136 R255Q and S441A mutants, generated additional cleavage bands in the spike, including a 100  
137 kDa band below the S2 band, which likely corresponds to the S2' fragment.

138 We then examined how the spike was cleaved by TMPRSS2 present on adjacent cells. To  
139 this aim, we mixed spike expressing cells with TMPRSS2 expressing cells. We assessed by  
140 western blot the processing of the spike 3 and 6 h after coculture (Extended Data Fig. 4b). The  
141 spike cleavage by WT TMPRSS2 was slightly visible 3 h after coculture, and this process was  
142 more marked at 6 h. Of note, syncytia were detected at 3 and 6 h post co-culture in the WT  
143 TMPRSS2 condition.

144 The WT and mutant TMPRSS2 had slightly different levels of expression upon transfection  
145 in 293T cells, when assessed by flow cytometry (Extended Data Fig. 4c, d). We thus adjusted  
146 the amounts of plasmids to reach similar levels. The catalytically inactive TMPRSS2 mutants  
147 barely induced cell-cell fusion with either HKU1A or B spikes (Fig. 2c), confirming the need  
148 of spike cleavage for cell-cell fusion.

149 We next generated single-cycle HKU1 pseudoviruses – lentiviral particles pseudotyped with  
150 HKU1 spikes – to further investigate the role of TMPRSS2 in HKU1 entry. The pseudovirus  
151 strategy has been successfully used to study SARS-CoV-2 entry and to identify ACE2 as a  
152 receptor for this virus<sup>37</sup>. HKU1A and B pseudoviruses did not infect parental 293T cells  
153 efficiently, while transient expression of TMPRSS2 enabled high viral entry (Fig. 2d).

154 In striking contrast with their inability to trigger cell-cell fusion, the catalytically inactive  
155 R255Q and S441A TMPRSS2 mutants readily allowed infection of 293T cells with HKU1A or  
156 HKU1B pseudovirus (Fig. 2d). The TMPRSS2 mutants behave as expected regarding the  
157 SARS-CoV-2 spike (D614G ancestral strain), which requires the enzymatic activity of the  
158 protease for infectivity enhancement<sup>37</sup>. In 293T-ACE2 cells, WT TMPRSS2 increased SARS-  
159 CoV-2 pseudotype entry by 8-fold, whereas this was not the case for the R255Q and S441A  
160 mutants (Extended Data Fig. 4e). Together, our data show that catalytic activity of TMPRSS2  
161 is not required for HKU1-mediated pseudovirus entry.

162 Coronavirus spike can either be processed by proteases at the surface of target cells, allowing  
163 for membrane fusion, or by cathepsins in endosomes, allowing for entry after internalization<sup>8</sup>.  
164 As TMPRSS2 catalytic activity was not required for HKU1 entry, we examined the cytoplasmic  
165 access route of pseudovirus in 293T cells expressing WT or S441A TMPRSS2. To this aim,  
166 we performed infections in presence of SB412515, a cathepsin L inhibitor, or E64d, a pan-

167 cysteine protease inhibitor. The drugs were added 2 h before infection and maintained for 48 h.  
168 SB412515 and E64d reduced the entry of HKU1A pseudovirus in S441A TMPRSS2 cells and  
169 not in WT TMPRSS2 cells (Extended Data Fig. 4f). This strongly suggests that viral entry  
170 occurs through endosomes with the catalytically inactive TMPRSS2 and at the surface with the  
171 WT protease. With HKU1B, SB412515 and E64d had little or no effect on entry (Extended  
172 Data Fig. 4g), suggesting that HKU1B might be cleaved by other proteases or requires less  
173 cleavage to induce fusion, although it still uses TMPRSS2 as a receptor. Infection by both  
174 HKU1A and HKU1B pseudoviruses was inhibited by hydroxychloroquine (HCQ) in S441A  
175 TMPRSS2 cells, confirming an endocytic route with the mutant protease (Extended Data Fig.  
176 4f, g).

177 We next asked whether TMPRSS2 could confer sensitivity to HKU1 pseudovirus in other  
178 cell lines. We generated U2OS and A549 stably expressing WT or S441A TMPRSS2. We  
179 reintroduced the two proteins in Caco2 TMPRSS2-KO cells. Flow cytometry demonstrated that  
180 TMPRSS2 was expressed in this panel of cells (Extended Data Fig. 4h, i). The presence of WT  
181 or S441A TMPRSS2 enabled infection to various extents of U2OS, A549 and Caco2 cells by  
182 HKU1A and HKU1B pseudoviruses (Fig. 2e). Knock-out of TMPRSS2 significantly reduced  
183 entry into Caco2 cells. Furthermore, in parental Caco2 cells, preincubation with Camostat, a  
184 serine protease inhibitor known to inhibit TMPRSS2, did not affect HKU1 pseudovirus  
185 infection, while, as expected, it diminished SARS-CoV-2 entry by two-fold (Extended Data Fig  
186 4j), confirming the role of endogenous TMPRSS2 as a receptor.

187 The Vero E6-TMPRSS2 cell line<sup>38</sup> remained insensitive to HKU1 pseudovirus infection  
188 (Extended Data Fig. 4k). Vero E6 cells are African green monkey kidney cells, it is thus  
189 possible that other parameters (glycosylation, sialylation, adhesion molecules or other cellular  
190 proteins, etc...) may regulate their sensitivity to HKU1.

191 We then analyzed the role of sialic acids during TMPRSS2-mediated HKU1 entry. We  
192 treated U2OS TMPRSS2+ cells with Neuraminidase, an enzyme that removes ( $\alpha$ 2,3), ( $\alpha$ 2,6)  
193 and ( $\alpha$ 2,8) linked sialic acids. Neuraminidase decreased binding of two sialic acid ligands,  
194 Lectin SNA and Siglec E, without affecting surface levels of TMPRSS2 (Extended data Fig.  
195 5). Neuraminidase reduced sensitivity of target cells to HKU1 pseudovirus infection in a dose-  
196 dependent manner, suggesting that sialic acids are necessary to trigger efficient HKU1 entry in  
197 TMPRSS2+ cells (Extended data Fig. 5).

198 Taken together, our results show that TMPRSS2 is required for HKU1 pseudovirus infection  
199 but that its catalytic activity is dispensable, possibly because it can be rescued by other proteases  
200 such as cathepsins.

201

## 202 **HKU1 spike binds to TMPRSS2**

203 We next generated recombinant ectodomains of HKU1A and B spikes to investigate their  
204 binding to TMPRSS2 expressing cells (Fig. 3a, b, Extended Data Fig. 6a). HKU1 spike bound  
205 weakly to WT TMPRSS2 and more strongly to TMPRSS2 S441A and R255Q, as assessed by  
206 flow cytometry. Addition of Camostat increased binding to WT TMPRSS2 (Fig. 3b, Extended  
207 Data Fig. 6a), indicating that the proteolytic activity of TMPRSS2 somehow interfered with our  
208 readout or decreased binding by degrading or shedding the bound spike. Alternatively, WT  
209 TMPRSS2's turnover might be faster than the mutants'. As expected, with a soluble SARS-  
210 CoV-2 spike, we detected binding to cells expressing ACE2 but not WT or mutant TMPRSS2  
211 (Fig. 3b, Extended Data Fig. 6a, b), highlighting the different behaviors of HKU1 and SARS-  
212 CoV-2.

213 We then showed binding of the recombinant TMPRSS2 ectodomain to the HKU1A or B  
214 spikes by ELISA, but not to the SARS-CoV-2 spike (Fig. 3c). This indicates a direct interaction  
215 between TMPRSS2 and the HKU1 spike. Conversely, soluble ACE2 bound the SARS-CoV-2  
216 but not the HKU1 spike by ELISA (Extended Data Fig. 6c). Due to the low yield of soluble  
217 WT TMPRSS2, we generated a soluble S441A mutant that could be obtained in amounts that  
218 allowed biophysical experiments. We expressed RBDs of the different viruses (residues 323-  
219 609 for HKU1A; 323-607 for HKU1B; 331-528 for SARS-CoV-2) to measure their affinity for  
220 S441A TMPRSS2 by biolayer interferometry (BLI). The RBDs from HKU1A and B interacted  
221 strongly with TMPRSS2, while the interaction of the SARS-CoV-2 RBD with TMPRSS2 was  
222 comparable to that of an irrelevant control protein (CD147) (Fig. 3d and Extended Data Fig.  
223 6d-e). Using a range of S441A TMPRSS2 concentrations, affinity constants ( $K_d$ ) of 334 nM  
224 and 137 nM were determined for HKU1A and B RBDs, respectively (Table 1, Extended Data  
225 Fig. 6d-e, SI 5, 6). The SARS-CoV-2 RBD bound to the ectodomain of ACE2 with a  $K_d$  of 92  
226 nM (Extended Data Fig. 6f, Table 1).

227

## 228 **HKU1 spike receptor binding motif**

229 The residues W515 and R517 within the HKU1 RBD<sup>19</sup> have been reported to be critical for  
230 binding to an unknown cellular receptor<sup>18</sup>. We produced the recombinant HKU1B RBD with  
231 the W515A or R517A mutations. As assessed by BLI, the W515A mutation abrogated  
232 interaction with TMPRSS2, reaching response levels comparable to those obtained with a  
233 control protein, while the R517A mutation reduced binding by 2.8-fold ( $K_d$ =376 nM) (Fig. 3e,  
234 Extended Data Fig. 6g, h, Table 1, SI 5, 6). We also generated plasmids coding for the HKU1A

235 and HKU1B spikes with the W515A or R517A mutations. These mutants were correctly  
236 expressed at the cell surface, as assessed by flow cytometry (Extended Data Fig. 6i) but they  
237 lost their cell-cell fusion properties in the presence of TMPRSS2 (Fig. 3f). Their ability to  
238 trigger pseudovirus entry was decreased by 2 to 3 logs, resulting in infection levels close to  
239 background (Fig. 3g). Therefore, the conserved W515 and R517 residues within the HKU1A  
240 and B RBDs are critical for binding to TMPRSS2, viral fusion and entry.

241

#### 242 **Anti-TMPRSS2 VHHs block spike binding**

243 We then examined whether the anti-TMPRSS2 VHH inhibited the HKU1 receptor function  
244 or the enzymatic activity of the protease. The 5 VHHs (A01, F05, A07, C11 and D01)  
245 efficiently bound soluble S441A TMPRSS2 as assessed by BLI (Extended Data Fig. 1a and  
246 Extended Data Table 1) and flow cytometry (Extended Data Fig. 7a). Three VHH (A07, C11  
247 and D01) inhibited the HKU1B RBD–interaction with S441A TMPRSS2 measured by BLI  
248 (Fig. 4a). The same three VHH reduced TMPRSS2 catalytic activity (Extended Data Fig. 7b).  
249 Those nanobodies also inhibited HKU1A and B spike – TMPRSS2 mediated cell-cell fusion  
250 (Fig. 4b, Extended Data Fig. 7c). We then examined their effect on viral entry independently  
251 of their inhibition of the catalytic activity of TMPRSS2. They reduced pseudovirus infection of  
252 293T cells expressing S441A TMPRSS2 in a dose-dependent manner (Fig. 4c, Extended Data  
253 Fig. 7d). The two other nanobodies (A01 and F05), despite showing efficient binding to  
254 TMPRSS2, did not interfere with its enzymatic activity and proviral roles (Fig. 4b, c and  
255 Extended Data Fig. 7c-d), suggesting that they bind to regions different from those of three  
256 active VHHs and that are not involved in HKU1 spike binding.

257

#### 258 **Anti-TMPRSS2 VHH blocks HKU1 infection**

259 HKU1 does not grow in any cell line tested up to date but viral amplification in human  
260 ciliated airway epithelial cell cultures has been reported<sup>29,39,40</sup>. We isolated an HKU1 virus from  
261 a nasal swab of an individual suffering from a respiratory tract infection. To this end, we used  
262 primary human bronchial epithelial cells (HBE cells) differentiated at the air/liquid interface  
263 (ALI) for over 4 weeks. We first examined whether these cells were positive for TMPRSS2.  
264 Immunofluorescence of HBE cells with the anti-TMPRSS2 VHH-A01-Fc revealed a  
265 preferential staining of ciliated cells, with a positive signal accumulating at the cilia (Fig. 5a).  
266 We then amplified the virus from the clinical sample by one passage on HBE cells. We observed  
267 an increase of HKU1 viral RNA in apical culture supernatants, with concentrations peaking at  
268  $5 \times 10^6$  viral RNA copies/ $\mu$ L at 2-3 days post-infection (dpi) (Extended Data Fig. 8a).

269 Metagenomic sequencing of the viral supernatant identified a HKU1 genotype B (Extended  
270 Data Fig. 8b), and no other virus was detected. For reasons that remain to be elucidated, our  
271 attempts to further grow this HKU1B isolate in various cell lines, expressing WT or S441  
272 TMPRSS2 were unsuccessful. However, the virus grew on a second passage on HBE cells,  
273 indicating that it was infectious (Extended Data Fig. 8a).

274 We then asked whether the anti-TMPRSS2 nanobodies inhibited infection of HBE cells. We  
275 preincubated target cells with the A07 VHH or a control nanobody and measured the spike  
276 intensity by immunofluorescence 48 h post-infection (Fig. 5b). The A07 VHH strongly reduced  
277 the appearance of infected cells, indicating that the spike binding and/or cleavage activities of  
278 TMPRSS2 are necessary for a productive HKU1 infection.

279

## 280 **Discussion**

281 Here, we demonstrate that TMPRSS2 is a receptor for HKU1. TMPRSS2 triggers HKU1-  
282 mediated cell-cell fusion, viral entry and binds with high affinity to both HKU1A and HKU1B  
283 RBDs. The enzymatic activity of TMPRSS2 is required for HKU1-dependent cell-cell fusion  
284 but not for entry of HKU1 pseudovirus. Two cathepsin inhibitors decrease HKU1A pseudovirus  
285 infection mediated by the catalytically inactive TMPRSS2, but not by the wild-type protease.  
286 This strongly suggests that after viral binding to TMPRSS2, viral particles expressing HKU1A  
287 can either fuse at the plasma membrane if the protease is active or be internalized and processed  
288 in the endosomal compartment when the protease is inactive. For HKU1B, other mechanisms  
289 could be at play.

290 TMPRSS2 directly binds to HKU1 but not to SARS-CoV-2 spikes. The autocleavage of  
291 TMPRSS2 is not required for binding. The affinity of HKU1A and HKU1B ( $K_d = 334$  and  $131$   
292 nM, respectively) is slightly below what we measured for the SARS-CoV-2 RBD interaction  
293 with ACE2 ( $K_d = 92$  nM). A conserved groove in a region of HKU1A and B spikes composed  
294 of amino acid 505, 515, 517-521 and 528 has been proposed to be involved in binding to an  
295 unknown receptor<sup>18,19</sup>. We show that the 515 and 517 residues of the spike are essential for  
296 efficient binding to TMPRSS2, viral fusion and entry, thus adding evidence that this region  
297 may be part of the RBM. Further structural studies are warranted to precisely map the amino-  
298 acids and regions allowing the interactions between the spike and its receptor. Another protease,  
299 Kalikrein 13 (KLK13) has been reported to cleave HKU1 spike<sup>41</sup>. Future work will help  
300 addressing how KLK13 may modulate HKU1 interaction with TMPRSS2.

301 We further designed anti-TMPRSS2 VHH that inhibit TMPRSS2 binding to HKU1 spikes  
302 and prevent cell-cell fusion and viral entry. The anti-TMPRSS2 nanobodies inhibit the

303 enzymatic activity of TMPRSS2 and hinder HKU1 pseudovirus entry using S441A TMPRSS2.  
304 This strongly suggests that the spike binds close to the catalytic site of the enzyme. These  
305 nanobodies confirmed the role of TMPRSS2 as a HKU1 receptor and provide useful tools to  
306 interfere with TMPRSS2 function. TMPRSS2 also plays a role in the development of certain  
307 cancers<sup>42</sup>. It will be worth studying how these nanobodies may target tumor cells or inhibit  
308 infection of viruses relying on this enzyme, as an alternative to small molecule inhibitors<sup>43</sup>.

309 Finally, we isolated an HKU1B live virus and report that TMPRSS2 is required for  
310 productive infection of primary HBE cells, that are natural targets of the virus. It will be of  
311 interest to further determine whether the HKU1 binding property, the enzymatic activity or  
312 most likely both functions of TMPRSS2 are necessary to trigger HKU1 infection in these  
313 primary cells. We were so far unable to amplify the virus in cell lines. Future work will be  
314 necessary to understand which step of the viral life cycle is impaired in TMPRSS2+ cell lines,  
315 or if another factor is required. It will be also worth examining whether soluble TMPRSS2,  
316 known to be shed in the extracellular space, may interfere with HKU1 entry.

317 Human coronavirus receptors that have been identified so far and allow productive viral  
318 entry are cell surface proteases. TMPRSS2 and other TTSP are known to prime human  
319 coronaviruses for fusion by cleaving their spikes, generally after viral binding to target cells.  
320 Of note, Omicron strains rely less on TMPRSS2 than previous SARS-CoV-2 lineages,  
321 reflecting a constant adaptation of coronaviruses to their hosts<sup>44</sup>. Our study provides the first  
322 evidence that TMPRSS2 also acts as a direct physical receptor for HKU1 entry, in addition to  
323 its previously known role in cleaving the spike. ACE2 binding is an ancestral and evolvable  
324 trait of sarbecoviruses<sup>45,46</sup>. TMPRSS2 binding may represent another parameter of coronavirus  
325 evolution. Whether coronaviruses have lost affinity or sensitivity to TMPRSS2 during  
326 evolution, or whether HKU1 has gained affinity for human or animal TMPRSS2 remains to be  
327 determined. Our results highlight the critical role of TMPRSS2 and other proteases as  
328 determinants of coronavirus tropism and pathogenesis<sup>23</sup>.

329

### 330 **Data availability**

331 Raw sequence data (human reads removed) for the HKU1 virus were deposited in the  
332 European Nucleotide Archive (ENA) portal (<https://www.ebi.ac.uk/ena/>) under bioproject  
333 accession number PRJEB64017. The raw data of the main figures are available within the  
334 supplementary information. The raw data of the extended data are available from the  
335 corresponding author upon reasonable request.

336

337 Supplementary Information is available for this paper.

338

339 Correspondence and requests for materials should be addressed to Olivier Schwartz.

340

341 Reprints and permissions information is available at [www.nature.com/reprints](http://www.nature.com/reprints).

342

### 343 **Author contributions**

344 Experimental strategy design: NS, IF, CP, MMR, HM, FR, JB, OS

345 Data acquisition and analysis: NS, IF, CP, VM, MMR, EBS, FP, FGB, JP, CB, AMa, LG,  
346 MOR, AMe, OA, HHW, MP, DD, ESL, JB

347 Vital materials and expertise: GCLF, MC, MD, VM, LVDH, PL

348 Manuscript writing: NS, JB, OS

349 Manuscript editing: NS, IF, CP, EBS, HM, FR, PL, JB, OS

350 All authors read and approved the final version of the manuscript.

351

### 352 **Acknowledgments**

353 We thank Ali Amara, Timothée Bruel and Nicoletta Casartelli for critical reading of the  
354 manuscript, members of the Virus and Immunity Unit for discussions and help, Nathalie  
355 Aulner, Nassim Mahtal and the UtechS Photonic BioImaging (UPBI) core facility (Institut  
356 Pasteur), Pierre Charneau for help in lentiviral pseudotype preparation, Stefan Pöhlmann for  
357 the kind gift of plasmids. NS is funded by the Ministère de l'Enseignement supérieur et de la  
358 Recherche. OS laboratory is funded by Institut Pasteur, Fondation pour la Recherche Médicale  
359 (FRM), ANRS-MIE, the Vaccine Research Institute (ANR-10-LABX-77), HERA European  
360 program (DURABLE consortium), Labex IBEID (ANR-10-LABX-62-IBEID), ANR/FRM  
361 Flash Covid PROTEO-SARS-CoV-2 and IDISCOVER. ESL lab is funded by the INCEPTION  
362 program (Investissements d'Avenir grant ANR-16-CONV-0005), the NIH PICREID program  
363 (Award Number U01AI151758), the HERA European program DURABLE (101102733) and  
364 the Labex IBEID (ANR-10-LABX-62-IBEID). HM laboratory is funded by the Institut Pasteur,  
365 the Milieu Intérieur Program (ANR-10-LABX-69-01), the INSERM, REACTing, and EU  
366 (RECOVER) grants. MMR was supported by the Pasteur-Paris University (PPU) International  
367 Doctoral Program and by Institut Pasteur Department of Virology "Bourse de Soudure"  
368 fellowship. FAR laboratory is funded by the French ANR (Agence Nationale de la Recherche),  
369 grants ANR-13-ISV8-0002-01, ANR-10-LABX-62-10 IBEID, Wellcome Trust collaborative  
370 grant (UNS22082), as well as by Institut Pasteur and CNRS. Work in UPBI is funded by grant

371 ANR-10-INSB-04-01 and Région Ile-de-France program DIM1-Health. The funders of this  
372 study had no role in study design, data collection, analysis and interpretation, or writing of the  
373 article.

374

### 375 **Conflict of interest**

376 NS, JB, OS, IF, EB, FAR, and PL have a provisional patent on anti-TMPRSS2 nanobodies.

377

378

### 379 **References**

380

- 381 1 Park, S., Lee, Y., Michelow, I. C. & Choe, Y. J. Global Seasonality of Human  
382 Coronaviruses: A Systematic Review. *Open Forum Infectious Diseases* 7 (2020).  
383 <https://doi.org:10.1093/ofid/ofaa443>
- 384 2 Bertram, S. *et al.* TMPRSS2 Activates the Human Coronavirus 229E for Cathepsin-  
385 Independent Host Cell Entry and Is Expressed in Viral Target Cells in the Respiratory  
386 Epithelium. *J. Virol.* **87**, 6150-6160 (2013). <https://doi.org:10.1128/jvi.03372-12>
- 387 3 Glowacka, I. *et al.* Evidence that TMPRSS2 Activates the Severe Acute Respiratory  
388 Syndrome Coronavirus Spike Protein for Membrane Fusion and Reduces Viral  
389 Control by the Humoral Immune Response. *J. Virol.* **85**, 4122-4134 (2011).  
390 <https://doi.org:10.1128/jvi.02232-10>
- 391 4 Shirato, K., Kawase, M. & Matsuyama, S. Wild-type human coronaviruses prefer cell-  
392 surface TMPRSS2 to endosomal cathepsins for cell entry. *Virology* **517**, 9-15 (2018).  
393 <https://doi.org:https://doi.org/10.1016/j.virol.2017.11.012>
- 394 5 Shirato, K., Kawase, M. & Matsuyama, S. Middle East respiratory syndrome  
395 coronavirus infection mediated by the transmembrane serine protease TMPRSS2. *J.*  
396 *Virol.* **87**, 12552-12561 (2013). <https://doi.org:10.1128/JVI.01890-13>
- 397 6 Milewska, A. *et al.* Human coronavirus NL63 utilizes heparan sulfate proteoglycans  
398 for attachment to target cells. *J. Virol.* **88**, 13221-13230 (2014).  
399 <https://doi.org:10.1128/JVI.02078-14>
- 400 7 Millet, J. K. & Whittaker, G. R. Host cell entry of Middle East respiratory syndrome  
401 coronavirus after two-step, furin-mediated activation of the spike protein. *Proc. Natl.*  
402 *Acad. Sci. U.S.A.* **111**, 15214-15219 (2014). <https://doi.org:10.1073/pnas.1407087111>
- 403 8 Shang, J. *et al.* Cell entry mechanisms of SARS-CoV-2. *Proc. Natl. Acad. Sci. U.S.A.*  
404 **117**, 11727-11734 (2020). <https://doi.org:10.1073/pnas.2003138117>
- 405 9 Shulla, A. *et al.* A Transmembrane Serine Protease Is Linked to the Severe Acute  
406 Respiratory Syndrome Coronavirus Receptor and Activates Virus Entry. *J. Virol.* **85**,  
407 873-882 (2011). <https://doi.org:doi:10.1128/JVI.02062-10>
- 408 10 Hofmann, H. *et al.* Human coronavirus NL63 employs the severe acute respiratory  
409 syndrome coronavirus receptor for cellular entry. *Proc. Natl. Acad. Sci. U.S.A.* **102**,  
410 7988-7993 (2005). <https://doi.org:10.1073/pnas.0409465102>
- 411 11 Curtis L. Yeager, R. A. A., Richard K. Williams, C. B. C. & Linda H. Shapirot, A. T.  
412 L., Kathryn V. Holmes. Human aminopeptidase N is a receptor for human coronavirus  
413 229E. *Nature* (1992).
- 414 12 Hulswit, R. J. G. *et al.* Human coronaviruses OC43 and HKU1 bind to 9-O-acetylated  
415 sialic acids via a conserved receptor-binding site in spike protein domain A. *Proc.*

- 416 *Natl. Acad. Sci. U.S.A.* **116**, 2681-2690 (2019).  
417 <https://doi.org/10.1073/pnas.1809667116>
- 418 13 Woo, P. C. Y. *et al.* Characterization and Complete Genome Sequence of a Novel  
419 Coronavirus, Coronavirus HKU1, from Patients with Pneumonia. *J. Virol.* **79**, 884-  
420 895 (2005). <https://doi.org/doi:10.1128/JVI.79.2.884-895.2005>
- 421 14 Kahn, J. S. & McIntosh, K. History and recent advances in coronavirus discovery.  
422 *Pediatr. Infect. Dis. J.* **24**, S223-227, discussion S226 (2005).  
423 <https://doi.org/10.1097/01.inf.0000188166.17324.60>
- 424 15 Sayama, Y. *et al.* Seroprevalence of four endemic human coronaviruses and, reactivity  
425 and neutralization capability against SARS-CoV-2 among children in the Philippines.  
426 *Sci Rep* **13**, 2310 (2023). <https://doi.org/10.1038/s41598-023-29072-3>
- 427 16 Killerby, M. E. *et al.* Human coronavirus circulation in the United States 2014-2017.  
428 *J. Clin. Virol.* **101**, 52-56 (2018). <https://doi.org/10.1016/j.jcv.2018.01.019>
- 429 17 Woudenberg, T. *et al.* Humoral immunity to SARS-CoV-2 and seasonal coronaviruses  
430 in children and adults in north-eastern France. *EBioMedicine* **70**, 103495 (2021).  
431 <https://doi.org/10.1016/j.ebiom.2021.103495>
- 432 18 Ou, X. *et al.* Crystal structure of the receptor binding domain of the spike glycoprotein  
433 of human betacoronavirus HKU1. *Nat Commun* **8**, 15216 (2017).  
434 <https://doi.org/10.1038/ncomms15216>
- 435 19 Kirchdoerfer, R. N. *et al.* Pre-fusion structure of a human coronavirus spike protein.  
436 *Nature* **531**, 118-121 (2016). <https://doi.org/10.1038/nature17200>
- 437 20 Bestle, D. *et al.* TMPRSS2 and furin are both essential for proteolytic activation of  
438 SARS-CoV-2 in human airway cells. *Life Science Alliance* **3**, e202000786 (2020).  
439 <https://doi.org/10.26508/lsa.202000786>
- 440 21 Huang, X. *et al.* Human Coronavirus HKU1 Spike Protein Uses O-Acetylated Sialic  
441 Acid as an Attachment Receptor Determinant and Employs Hemagglutinin-Esterase  
442 Protein as a Receptor-Destroying Enzyme. *J. Virol.* **89**, 7202-7213 (2015).  
443 <https://doi.org/doi:10.1128/JVI.00854-15>
- 444 22 Li, Z. *et al.* Synthetic O-acetylated sialosides facilitate functional receptor  
445 identification for human respiratory viruses. *Nat Chem* **13**, 496-503 (2021).  
446 <https://doi.org/10.1038/s41557-021-00655-9>
- 447 23 Millet, J. K., Jaimes, J. A. & Whittaker, G. R. Molecular diversity of coronavirus host  
448 cell entry receptors. *FEMS Microbiol. Rev.* **45** (2020).  
449 <https://doi.org/10.1093/femsre/fuaa057>
- 450 24 Bugge, T. H., Antalis, T. M. & Wu, Q. Type II transmembrane serine proteases. *J.*  
451 *Biol. Chem.* **284**, 23177-23181 (2009). <https://doi.org/10.1074/jbc.R109.021006>
- 452 25 Fraser, B. J. *et al.* Structure and activity of human TMPRSS2 protease implicated in  
453 SARS-CoV-2 activation. *Nat. Chem. Biol.* **18**, 963-971 (2022).  
454 <https://doi.org/10.1038/s41589-022-01059-7>
- 455 26 Böttcher-Friebertshäuser, E. Membrane-Anchored Serine Proteases: Host Cell Factors  
456 in Proteolytic Activation of Viral Glycoproteins. *Activation of Viruses by Host*  
457 *Proteases*, 153-203 (2018). [https://doi.org/10.1007/978-3-319-75474-1\\_8](https://doi.org/10.1007/978-3-319-75474-1_8)
- 458 27 Fraser, B. J. *et al.* Structure and activity of human TMPRSS2 protease implicated in  
459 SARS-CoV-2 activation. *Nat. Chem. Biol.* **18**, 963-971 (2022).  
460 <https://doi.org/10.1038/s41589-022-01059-7>
- 461 28 Lukassen, S. *et al.* SARS-CoV-2 receptor ACE2 and TMPRSS2 are primarily  
462 expressed in bronchial transient secretory cells. *The EMBO Journal* **39**, e105114  
463 (2020). [https://doi.org:https://doi.org/10.15252/embj.20105114](https://doi.org/https://doi.org/10.15252/embj.20105114)

- 464 29 Pyrc, K. *et al.* Culturing the Unculturable: Human Coronavirus HKU1 Infects,  
465 Replicates, and Produces Progeny Virions in Human Ciliated Airway Epithelial Cell  
466 Cultures. *J. Virol.* **84**, 11255-11263 (2010). <https://doi.org/doi:10.1128/JVI.00947-10>
- 467 30 Planchais, C. *et al.* Potent human broadly SARS-CoV-2–neutralizing IgA and IgG  
468 antibodies effective against Omicron BA.1 and BA.2. *J. Exp. Med.* **219** (2022).  
469 <https://doi.org:10.1084/jem.20220638>
- 470 31 Buchrieser, J. *et al.* Syncytia formation by SARS-CoV-2-infected cells. *EMBO J.* **39**,  
471 e106267 (2020). <https://doi.org:10.15252/embj.2020106267>
- 472 32 Zang, R. *et al.* TMPRSS2 and TMPRSS4 promote SARS-CoV-2 infection of human  
473 small intestinal enterocytes. *Sci Immunol* **5** (2020).  
474 <https://doi.org:10.1126/sciimmunol.abc3582>
- 475 33 Kishimoto, M. *et al.* TMPRSS11D and TMPRSS13 Activate the SARS-CoV-2 Spike  
476 Protein. *Viruses* **13** (2021). <https://doi.org:10.3390/v13030384>
- 477 34 Hoffmann, M. *et al.* Camostat mesylate inhibits SARS-CoV-2 activation by  
478 TMPRSS2-related proteases and its metabolite GBPA exerts antiviral activity.  
479 *EBioMedicine* **65**, 103255 (2021).  
480 <https://doi.org:https://doi.org/10.1016/j.ebiom.2021.103255>
- 481 35 Koch, J. *et al.* TMPRSS2 expression dictates the entry route used by SARS-CoV-2 to  
482 infect host cells. *The EMBO Journal* **40**, e107821 (2021).  
483 <https://doi.org:https://doi.org/10.15252/embj.2021107821>
- 484 36 Daniel E. H. Afar *et al.* Catalytic Cleavage of the Androgen-regulated TMPRSS2  
485 Protease Results in Its Secretion by Prostate and Prostate Cancer Epithelia. *Cancer*  
486 *Res.* **31**, 1686-1692 (2001).
- 487 37 Hoffmann, M. *et al.* SARS-CoV-2 Cell Entry Depends on ACE2 and TMPRSS2 and  
488 Is Blocked by a Clinically Proven Protease Inhibitor. *Cell* **181**, 271-280.e278 (2020).  
489 <https://doi.org:https://doi.org/10.1016/j.cell.2020.02.052>
- 490 38 Planas, D. *et al.* Resistance of Omicron subvariants BA.2.75.2, BA.4.6, and BQ.1.1 to  
491 neutralizing antibodies. *Nature Communications* **14**, 824 (2023).  
492 <https://doi.org:10.1038/s41467-023-36561-6>
- 493 39 Dominguez, S. R. *et al.* Isolation, propagation, genome analysis and epidemiology of  
494 HKU1 betacoronaviruses. *J. Gen. Virol.* **95**, 836-848 (2014).  
495 <https://doi.org:https://doi.org/10.1099/vir.0.059832-0>
- 496 40 Dijkman, R. *et al.* Isolation and Characterization of Current Human Coronavirus  
497 Strains in Primary Human Epithelial Cell Cultures Reveal Differences in Target Cell  
498 Tropism. *J. Virol.* **87**, 6081-6090 (2013). <https://doi.org:doi:10.1128/JVI.03368-12>
- 499 41 Milewska, A. *et al.* Kallikrein 13 serves as a priming protease during infection by the  
500 human coronavirus HKU1. *Science Signaling* **13**, eaba9902 (2020).  
501 <https://doi.org:10.1126/scisignal.aba9902>
- 502 42 Koistinen, H. *et al.* The roles of proteases in prostate cancer. *IUBMB Life*  
503 <https://doi.org:https://doi.org/10.1002/iub.2700>
- 504 43 Shrimp, J. H. *et al.* An Enzymatic TMPRSS2 Assay for Assessment of Clinical  
505 Candidates and Discovery of Inhibitors as Potential Treatment of COVID-19. *ACS*  
506 *Pharmacology & Translational Science* **3**, 997-1007 (2020).  
507 <https://doi.org:10.1021/acsptsci.0c00106>
- 508 44 Suzuki, R. *et al.* Attenuated fusogenicity and pathogenicity of SARS-CoV-2 Omicron  
509 variant. *Nature* **603**, 700-705 (2022). <https://doi.org:10.1038/s41586-022-04462-1>
- 510 45 Li, W. *et al.* Angiotensin-converting enzyme 2 is a functional receptor for the SARS  
511 coronavirus. *Nature* **426**, 450-454 (2003). <https://doi.org:10.1038/nature02145>
- 512 46 Starr, T. N. *et al.* ACE2 binding is an ancestral and evolvable trait of sarbecoviruses.  
513 *Nature* **603**, 913-918 (2022). <https://doi.org:10.1038/s41586-022-04464-z>

514

515 **Figure Legends**

516

517 **Figure 1. TMPRSS2 triggers HKU1 spike fusion. a. Alignment of HKU1A and B spikes.**  
518 NTD: N-terminal Domain. CTD: C-terminal domain. FP: Fusion-peptide. HR1/2: Heptad-  
519 Repeat 1/2. TMD: Transmembrane Domain. Black: mismatch, white: deletion, boxed text  
520 (Red): amino-acids of the putative RBM, S1/S2 and S2/S2' cleavage site. **b. TMPRSS2**  
521 **mediates HKU1 cell-cell fusion.** 293T cells expressing either GFP1-10 or GFP11 (293T-GFP-  
522 split cells) were transfected with HKU1 spike and TMPRSS2 or pQCXIP-empty control (Ctrl)  
523 plasmids, fusion was quantified by measuring the GFP area after 20 h. Data are mean  $\pm$  SD of  
524 5 independent experiments. **c. Effect of a panel of proteases on cell-cell fusion.** 293T-GFP-  
525 split cells were transfected with HKU1 spike and the indicated protease plasmids, fusion was  
526 quantified by measuring the GFP area after 48 h. Data are mean  $\pm$  SD of 3 independent  
527 experiments. **d. TMPRSS2 has to be on the acceptor cell.** TMPRSS2 was transfected either  
528 in donor cells and HKU1A spike or in acceptor cells. Fusion was quantified after 20 h. Left:  
529 experimental design. Middle: representative images of GFP+ cells. Right: fusion quantification.  
530 bar: 400  $\mu$ m. Data are mean  $\pm$  SD of 4 independent experiments. **e. Role of endogenous**  
531 **TMPRSS2.** 293T donor cells expressing HKU1A spike were mixed with Caco2 acceptor cells  
532 knocked-out or not for the *tmprss2* gene. Left: experimental design. Middle: representative  
533 images of GFP+ cells. Right: fusion was quantified by measuring the GFP area after 20 h of  
534 coculture. Data are mean  $\pm$  SD of 3 independent experiments. **Statistical analysis:** b, d, e: Two-  
535 sided unpaired t-test compared to control/parental condition. c: one Way ANOVA on non-  
536 normalized data with Tukey's multiple comparisons.

537

538 **Figure 2. Effect of wild-type and mutant TMPRSS2 on HKU1 cell-cell fusion and**  
539 **pseudovirus infection. a. TMPRSS2 protein.** TMPRSS2 is composed of a Transmembrane  
540 Domain (TMD), a class A LDL receptor domain (LDLR), a Scavenger Receptor Cysteine-2  
541 rich domain (SRCRD) and a serine peptidase. TMPRSS2 precursor autocleaves at R255-L256,  
542 resulting in an active protease. **b. TMPRSS2 and spike cleavage.** WB of 293T transfected with  
543 HKU1A spike and indicated TMPRSS2 mutants. One membrane was probed for S1, TMPRSS2  
544 and actin, another for S2 and actin. For gel source data, see SI 1a, b. Representative blots of 3  
545 independent experiments. Molecular weights: kDa. Arrows and # denote the uncleaved and  
546 cleaved proteins, respectively. **c. Catalytically inactive TMPRSS2 mutants do not trigger**  
547 **HKU1 cell-cell fusion.** Fusion of 293T-GFP split transfected with HKU1 spike and mutant  
548 TMPRSS2 was quantified after 20 h and normalized to WT TMPRSS2. Ctrl: pQCXIP-Empty.  
549 Left: HKU1A. Right: HKU1B. Data are mean  $\pm$  SD of 3 independent experiments. **d.**  
550 **Catalytically inactive TMPRSS2 mutants mediate HKU1 pseudovirus infection.** 293T  
551 transfected with WT or mutant TMPRSS2 were infected by Luc-encoding HKU1 pseudovirus.  
552 Luminescence was read 48 h post infection. Dotted line indicates background in non-infected  
553 cells. Ctrl: pQCXIP-Empty. Data are mean  $\pm$  SD of 6 (HKU1A) or 3 (HKU1B) independent  
554 experiments. **e. HKU1 pseudovirus infection in cell lines stably expressing TMPRSS2.** Left:  
555 U2OS cells. Middle: A549 cells. Right: Caco2 cells. The TMPRSS2 KO Caco2 cells were  
556 stably transduced with indicated TMPRSS2. Data are mean  $\pm$  SD of 3 (U2OS), 8 (A549), 4  
557 (Caco2) independent experiments. **Statistical analysis:** c: one-way ANOVA on non-  
558 normalized data with Dunnett's multi-comparison test compared to WT TMPRSS2 expressing  
559 cells. d, e: one-way ANOVA on log-transformed data with Dunnett's multi-comparison test

560 compared to the untransfected (d), parental (e: U2OS and A549) or KO cells (e: Caco2),  
561 \*\*\*p<0.0001.

562

563 **Figure 3. Analysis of HKU1 spike binding to TMPRSS2. a-b. Binding of soluble HKU1**  
564 **spikes to 293T cells expressing TMPRSS2.** Cells were transfected with TMPRSS2 mutants  
565 and incubated or not with 10  $\mu$ M of Camostat. **a. TMPRSS2 levels** (assessed with a commercial  
566 Ab) **b. Binding of soluble biotinylated trimeric spikes** measured by flow cytometry. One  
567 representative experiment of 3 is shown. Ctrl: pQCXIP-Empty control plasmid. **c. Binding of**  
568 **HKU and SARS-CoV-2 spikes on immobilized WT TMPRSS2 measured by ELISA.** Mean  
569 of 2 independent experiments. **d. Binding of S441A TMPRSS2 to RBD coated receptors**  
570 **quantified by Bio-layer interferometry (BLI).** One representative experiment of 4 is shown.  
571 **e, f, g. Properties of W515A and R517A mutant HKU1 spikes.** Binding of TMPRSS2 to  
572 wild type or mutant RBD coated receptors quantified by BLI. One representative experiment  
573 of 4 is shown. **f.** 293T GFP-split cells were transfected with TMPRSS2 and the indicated HKU1  
574 mutant spikes, fusion was quantified by measuring the GFP area after 24 h. **g.** 293T cells  
575 expressing TMPRSS2 were infected by Luc-encoding mutant HKU1 pseudovirus.  
576 Luminescence was read 48 h post infection. Dotted line indicates background. Data are mean  
577  $\pm$  SD of 3 independent experiments. **Statistical analysis:** f: one-way ANOVA on non-  
578 normalized data with Dunnett's multi-comparison test compared to WT TMPRSS2 expressing  
579 cells. g: one-way ANOVA on log-transformed data with Dunnett's multi-comparison test  
580 compared to WT Spike pseudotypes \*p<0.05, \*\*p<0.01, \*\*\*p<0.001.

581

582 **Figure 4. Anti-TMPRSS2 VHH nanobodies inhibit HKU1 binding to TMPRSS2, cell-cell**  
583 **fusion and pseudovirus infection. a. Effect of VHHs on binding of HKU1B RBD to**  
584 **TMPRSS2 measured by BLI.** One representative experiment of 2 is shown **b. Effect of VHHs**  
585 **on HKU1-mediated cell-cell fusion.** 293T GFP-Split cells were transfected with TMPRSS2  
586 and HKU1 spike in the presence of 1  $\mu$ M of VHH, fusion was quantified 20 h later. Data were  
587 normalized to the non-VHH treated condition (dotted line). Data are mean  $\pm$  SD of 4  
588 independent experiments. **c. Effect of VHHs on HKU pseudovirus infection.** 293T cells  
589 transfected with S441A TMPRSS2 were treated with 1  $\mu$ M VHH 2 h before infection.  
590 Luminescence was read 48 h post infection. Data were normalized to the non-treated condition  
591 for each virus (dotted line). Data are mean  $\pm$  SD of 3 independent experiments. **Statistical**  
592 **analysis:** b: one Way ANOVA data with Dunnett's multiple comparisons compared to non-  
593 target VHH c: one Way ANOVA on log-transformed data with Dunnett's multiple comparisons  
594 compared to non-target VHH \*p<0.05, \*\*p<0.01, \*\*\*p<0.001. p-values. Fusion, HKU1A: A07  
595 0.0005, C11: 0.025, D01: 0.004, HKU1B: A07: 0.029, Infection: HKU1A: A01: 0.016, A07:  
596 <0.0001, C11:0.0009, D01:<0.0001 HKU1B: A07/C11/D01: <0.0001

597

598

599 **Figure 5. Live HKU1 virus infection of human bronchial epithelial (HBE) cells. a.**  
600 **TMPRSS2 staining of HBE cells.** Red: Phalloidin, Blue: DAPI, Green: TMPRSS2 stained  
601 with VHH A01-Fc. Scale bars: top, 10  $\mu$ m; bottom, 5  $\mu$ m. Images are representative of 3  
602 independent experiments. **b. Effect of the anti-TMPRSS2 VHH (A07) on HKU1 infection.**  
603 The experimental design is represented. Infected cells were visualized with an anti-spike  
604 antibody and scored. Representative images of spike staining 48 h post-infection are shown.  
605 Spike pixel intensity in 5 random fields per experiment was measured and normalized to the  
606 intensity in the infected but non-treated condition. Data are mean  $\pm$  SD of 3 independent  
607 experiments for infected conditions, and mean of 2 for uninfected condition. Scale bar: 20  $\mu$ m.  
608 **Statistical analysis:** Two-sided unpaired t-test compared to non-target VHH.

609

610 **Table 1:** Affinity ( $K_d$ ) of the indicated RBD for TMPRSS2 or ACE2. ND (Non-Detectable)  
611 denotes proteins for which interaction with the loaded sensor was similar or below the  
612 interaction with an empty sensor.

613

614

615

## 616 **Methods**

### 617 **Plasmids**

618 Codon-optimized HKU1A (RefSeq: YP\_173238.1) and B/C isolate N5P8, referred to  
619 HKU1B (UniProtKB/Swiss-Prot: Q0ZME7.1) full spikes were ordered as synthetic genes  
620 (GeneArt, Thermo Fisher Scientific) and cloned into a phCMV backbone (GeneBank:  
621 AJ318514), by replacing the VSV-G gene. pQCXIP-Empty control plasmid was previously  
622 described<sup>31</sup>. pQCXIP-BSR-GFP11 and pQCXIP-GFP1-10 were a kind gift from Yutaka Hata<sup>47</sup>  
623 (Addgene plasmid #68716 and #68715). pCSDest-TMPRSS2 was a kind gift from Roger  
624 Reeves<sup>48</sup> (Addgene plasmid # 53887). Mutations in the HKU1 spike and TMPRSS2 were  
625 introduced using the NEB Q5 Side-Directed mutagenesis kit. Plasmids were sequenced before  
626 usage. phCMV-HKU1-S-mNeonGreen and pCDEST-TMPRSS2-mScarlet-I were generated by  
627 Gibson assembly. pCAGGS-based expression vectors N-terminal cMYC-epitope tagged  
628 TMPRSS2, TMPRSS3, TMPRSS4, TMPRSS10, TMPRSS11A, TMPRSS11B, TMPRSS11D,  
629 TMPRSS11E, TMPRSS11F and TMPRSS13 were a kind gift from Stefan Pöhlmann<sup>34</sup>. pLV-  
630 EF1a-IRES-Hygro was a gift from Tobias Meyer (Addgene plasmid # 85134)<sup>49</sup>. pLV-EF1a-  
631 DEST-IRES-Hygro was generated by Gibson assembly. pLV-TMPRSS2-Hygro was generated  
632 by cloning TMPRSS2 from pCSDest-TMPRSS2 into pLV-EF1a-DEST-IRES-Hygro using  
633 gateway cloning. pLV-TMPRSS2-S441A-Hygro and pLV-TMPRSS2-R255Q-Hygro were  
634 generated by Q5 site directed mutagenesis (New England Biolabs).

635

### 636 **Cells**

637 HEK293T (293T), U2OS, VeroE6, A549 and Caco2/TC7 (Caco2) were from ATCC and  
638 cultured in DMEM with 10% fetal bovine serum (FBS) and 1% penicillin/streptomycin (PS).  
639 GFP-split cells were previously described<sup>31</sup> and cultured with 1  $\mu\text{g}/\text{mL}$  of puromycin  
640 (InvivoGen). Cells stably expressing TMPRSS2 were cultured with 100  $\mu\text{g}/\text{mL}$  hygromycin.  
641 Cells were routinely screened for mycoplasma. Cells were authenticated by genotyping  
642 (Eurofins).

643

644 **Reagents**

645 SB412515 was purchased from Cayman Chemical, E64d and Camostat mesylate from  
646 Sigma Aldrich, hydroxychloroquine from Merck, Neuraminidase (or Sialidase from  
647 *Arthrobacter ureafaciens*) from Roche.

648

649 **Sequence alignments**

650 Alignments of HKU1 A and B spikes in Fig. 1a were performed using Protein Blast with  
651 default settings (NCBI). Alignment figures were generated using the seqvisr package in R  
652 (Github: 10.5281/zenodo.6583981).

653

654 **GFP-split fusion assay**

655 Cell-cell fusion assays were performed as previously described<sup>31,50</sup>. Briefly, 293T cells  
656 stably expressing GFP1-10 and GFP11 were co-cultured at a 1:1 ratio ( $6 \times 10^4$  cells/well) and  
657 transfected in suspension with Lipofectamine 2000 (Thermo) in a 96-well plate (uClear,  
658 #655090) (10 ng of spike plasmid, indicated amounts of TMPRSS2 plasmids adjusted to 100 ng  
659 DNA with pQCXIP-Empty). For Acceptor-Donor experiments, 293T GFP-split cells (GFP1-  
660 10 and GFP11) were transfected separately in suspension with 500 ng of DNA (10% spike,  
661 indicated amounts of TMPRSS2 plasmid adjusted to 500 ng with pQCXIP-Empty) for 30 min  
662 at 37°C. Cells were washed twice and acceptor and donor cells were mixed and seeded at  $6$   
663  $\times 10^4$  cells/well. For Caco2 KD experiments, Caco2 GFP11 cells were transfected with control  
664 siRNA-directed against Luciferase: 5'-CGUACGCGGAAUACUUCGA-3' or siGENOME  
665 Human TMPRSS2 SMARTpool (#7113 - Horizon Discovery) at 50 nM using Lipofectamine™  
666 RNAiMAX (Thermo Fisher Scientific) in a 6 well dish for 48 h. 293T GFP1-10 cells were  
667 transfected with 10% of spike plasmid in a 6 well dish for 24 h. Caco2 KD or Caco2 KO cells  
668 and 293T spike cells were mixed at a 1:1.5 ratio in a 96 well plate. The remaining Caco2 cells  
669 were used for RNA extraction for qPCR. For all experiments, at 20 h post-transfection, images  
670 covering 90% of the well surface, were acquired per well on an Opera Phenix High-Content  
671 Screening System (PerkinElmer). The GFP area was quantified on Harmony High-Content  
672 Imaging and Analysis Software.

673

674 **RNA Extraction, Reverse Transcription, and qPCR**

675 At 48 h post siRNA transfection,  $5 \times 10^5$  Caco2 cells were lysed using RLT buffer  
676 (QIAGEN) supplemented with 10  $\mu$ L of  $\beta$ -mercaptoethanol. RNA extraction was performed  
677 using the RNeasy plus mini kit (QIAGEN) according to the manufacturer's protocol. Reverse

678 transcription was performed using SuperScript II (Thermo Fisher Scientific) according to the  
679 manufacturer's protocol. qPCR was performed using iTaq universal SYBR green supermix (Bio  
680 Rad) on a QuantStudio 6 Real-Time PCR machine (Thermo Fisher Scientific). The following  
681 primers were used:  $\beta$ -Tubulin forward: 5'-CTTCGGCCAGATCTTCAGAC-3', reverse: 5'-  
682 AGAGAGTGGGTCAGCTGGAA-3'; TMPRSS2 forward: 5'-  
683 GGGGATACAAGCTGGGGTTC-3', reverse: 5'-GATTAGCCGTCTGCCCTCAT-3'.

684

#### 685 **HKU1-spike-TMPRSS2 video microscopy**

686 One million 293T cells were transfected either with 1  $\mu$ g of pCDEST-TMPRSS2-scarlet-I or  
687 phCMV-HKU1A S-NeonGreen plasmid in a 6-well plate using lipofectamine 2000 according  
688 to the manufacturer's protocol. At 24 h post transfection, cells were harvested with PBS + 0.1%  
689 EDTA and resuspended at  $6 \times 10^5$  cells/mL in DMEM 10% FCS. The cells were mixed in  
690 suspension at a 50/50 ratio and 100  $\mu$ L were plated per well in a 96-well plate (uClear,  
691 #655090). 30 min after plating, cells were imaged every 150 sec for 2.5 h at 37°C, 5% CO<sub>2</sub> on  
692 an Opera Phenix High-Content Screening System (PerkinElmer).

693

#### 694 **Pseudovirus generation and infection**

695 Pseudoviruses were produced by transfection of 293T cells as previously described<sup>51</sup>.  
696 Briefly, cells were cotransfected with plasmids encoding for lentiviral proteins, a luciferase  
697 reporter, and the HKU1 spike plasmid. Pseudotyped virions were harvested 2 and 3 days after  
698 transfection. Production efficacy was assessed by measuring infectivity or HIV Gag p24  
699 concentration. For transfected cells (293T), infection was performed 24 h post-transfection, in  
700 suspension using 10 ng of p24 and  $2 \times 10^4$  cells in 100  $\mu$ L. For the stable cell lines, infection  
701 was performed on plated cells, with or without spinoculation (2 h at 2000 g), using 10-50 ng of  
702 p24 per well and  $2 \times 10^4$  cells in 100  $\mu$ L in a 96 well plate. The next day, 100  $\mu$ L of media was  
703 added. 48 h post-infection, 100  $\mu$ L of media was carefully removed, and 100  $\mu$ L of Bright-  
704 Glo™ lysis buffer (ProMega) was added. After 10 min, luminescence was acquired using the  
705 EnSpire in a white plate (PerkinElmer).

706

#### 707 **Isolation and characterization of a live HKU-1 virus**

##### 708 *Origin of the sample*

709 Respiratory material of sample MAL21 0303 was obtained in the winter of 2022-2023 at  
710 Amsterdam UMC. Material was collected in Universal Transport Medium (Copan) and stored  
711 at -80°C. Details on the disease of the patient are unknown as material were donated for research

712 anonymously. Presence of HCoV-HKU1 was determined via real time qPCR as described <sup>52</sup>  
713 with primers: HKU1 forward: 5'-TCCTACTAYTCAAGAAGCTATCC-3'; HKU1 reverse 5'-  
714 AATGAACGATTATTGGGTCCAC-3'; and HKU1-probe CY5 BHQ2  
715 TYCGCCTGGTACGATTTTGCCTCA.

716

#### 717 *HKU1 isolation and culture on Human nasal epithelium*

718 MucilAir<sup>TM</sup>, reconstructed human nasal epithelium cultures that had been differentiated for  
719 4 weeks were purchased from Epithelix (Saint-Julien-en-Genevois, France) and were cultured  
720 in 700 µL MucilAir<sup>TM</sup> media on the basal side of the air/liquid interface (ALI) cultures and  
721 monitored for healthy cilia movements. Cultures were kept at 34°C under a 5% CO<sub>2</sub>  
722 atmosphere. One-hour prior to infection, mucus was removed from the apical side of the culture  
723 by washing with HBSS (Gibco). For viral isolation, cells were infected with nasal swabs diluted  
724 at a 1:4 ratio in universal transport medium (Copan) for 2 h at 34°C. Viral input was removed  
725 and cells were washed three times with 200 µL of HBSS (Gibco). Apical side was harvested  
726 twice every 24 h for 7 days by adding 200 µL HBSS for 10 min at 34°C and collecting the  
727 liquid on the apical side and diluting it (1:1) in virus transport medium (Copan). The harvest  
728 was centrifuged at 1000 g for 5 min to remove debris, 50 µL was used for qPCR and the  
729 remaining samples were stored at -80°C. Passage 1 (P1) and P2 viral stocks were sequenced  
730 with identical results.

731

#### 732 *Sequencing of the HKU1 strain*

733 RNA was extracted from the cell supernatant using the QIAamp Viral RNA kit (Qiagen)  
734 following the manufacturer instructions. Extracted RNA was treated with Turbo DNase  
735 (Ambion) followed by ribosomal RNA<sup>53</sup>. RNA was reverse-transcribed into double stranded  
736 cDNA using random hexamers, and libraries prepared using the Nextera XT kit (Illumina),  
737 before sequencing on an Illumina NextSeq500 (2 × 75 cycles). Raw sequence data (human  
738 reads removed) were deposited in the European Nucleotide Archive (ENA) portal  
739 (<https://www.ebi.ac.uk/ena/>) under bioproject accession number PRJEB64017. To determine  
740 the sequence of the acidic tandem repeat region of the genome, the region was amplified using  
741 external primers (HKU1\_ATR\_L1 5'-ATGAAGCAATGGCCTCTCGT-3' and  
742 HKU1\_ATR\_R1 5'-CACAGAACGCAACCAACAGT-3'), before Sanger sequencing.

#### 743 *Genome assembly*

744 Adapters and low-quality sequences of raw reads were removed using Trimmomatic v0.39<sup>54</sup>.  
745 We assembled the trimmed reads using megahit v1.2.9<sup>55</sup> with default parameters. The contigs  
746 were queried against the NCBI non-redundant protein database using DIAMOND v2.0.4<sup>56</sup>, to  
747 look for potential contaminants in addition to the detected HKU1 genome. The Sanger data was  
748 used with the assembled contigs to generate the final HKU1 scaffold, on which the trimmed  
749 reads were mapped to generate the final consensus (Extended Data Fig. 8). The mapping data  
750 was visually checked to confirm the accuracy of the obtained genome using Geneious Prime  
751 2023. The sequence of the isolated virus was deposited in GenBank, ID: HCoV-  
752 HKU1/NDL/IPP01/2022, accession number OR260091.

### 753 *Phylogenetic and recombination analysis*

754 All available complete HKU1 genome sequence data and metadata were retrieved from BV-  
755 BRC (PMID: 36350631) (<https://www.bv-brc.org/>) in June 2023. Sequences were aligned  
756 using MAFFT (v.7.467)<sup>57</sup> and the alignment was checked for accuracy using BioEdit v7.2.5.  
757 We used a combination of six methods implemented in RDP4<sup>58</sup> (RDP, GENECONV, MaxChi,  
758 Bootscan, SisScan, and 3SEQ) to detect potential recombination events in the newly reported  
759 genome. The ModelFinder application<sup>59</sup>, as implemented in IQ-TREE v2.0.6 (PMID:  
760 25371430), was used to select the best-fitting nucleotide substitution model, and maximum-  
761 likelihood phylogenies were inferred using complete genomes or the spike coding sequences.  
762 Branch support was calculated using ultrafast bootstrap approximation with 1000 replicates<sup>60</sup>.  
763 The phylogenies were visualized using the auspice module from Nextstrain<sup>61</sup>. Interactive  
764 phylogenies are available at: <https://github.com/Simon-LoriereLab/HKU1>

765

### 766 **Analysis of HKU-1 replication by RT qPCR**

767 Viral RNA was extracted from culture supernatants using the Quick-DNA/RNA Viral 96  
768 Kit (Zymo) according to manufacturer's instructions. qPCR was run using the Luna Universal  
769 Probe One-Step kit on a QuantStudio6 (Thermo) according to manufacturer's instructions using  
770 the following primers (HKUqPCR5: 5'-CTGGTACGATTTTGCCTCAA-3') and  
771 (HKUqPCR3: 5'-ATTATTGGGTCCACGTGATTG-3')<sup>29</sup> and TaqMan™ QSY probe (5'-  
772 FAM-TTGAAGGCTCAGGAAGGTCTGCTTCTAA-QSY7-3'). A DNASring was used for  
773 generating a standard curve (5'-  
774 GGATCCTACTATTCAAGAAGCTATCCCTACTAGGTTTTTCGCCCTGGTACGATTTTGC  
775 CTCAAGGCTATTATGTTGAAGGCTCAGGAAGGTCTGCTTCTAATAGCCGCCAGG

776 TTCACGTTCTCAATCACGTGGACCCAATAATCGTTCATTAAGTAGAAGTAATTCT  
777 AATTTTAGACATTCTGATTCTATAGTGAAACCTG-3')

778

### 779 **Human nasal epithelium VHH inhibition experiments**

780 One hour prior to infection, mucus was removed from the apical side of the culture by  
781 washing with HBSS (Gibco). For viral infectivity assays, cells were incubated for 30 min with  
782 50  $\mu$ L of universal transport media (Yocon), containing monomeric non-target VHH93 (also  
783 termed N-G9-3<sup>62</sup>) or anti-TMPRSS2 VHH A07 at 5  $\mu$ M. Then  $5 \times 10^6$  viral copies were added  
784 in 50  $\mu$ L of universal transport medium for 2 h at 34°C (final VHH of concentration 2.5  $\mu$ M).  
785 Viral input was removed and cells were washed three times with 200  $\mu$ L of HBSS (Gibco).  
786 After 48 h, cells were fixed on the apical and basal sides with 4% PFA for 30 min. For imaging,  
787 fixed cells were stained intracellularly with mAb10 at 1  $\mu$ g/mL a pan anti-coronavirus spike  
788 antibody<sup>30</sup>, anti-TMPRSS2 VHH-A01-Fc at 6  $\mu$ g/mL and phalloidin Atto-647 (Sigma-aldrich)  
789 at 1:200 as described previously<sup>63</sup> and imaged using the LSM-700 confocal microscope (Zeiss).

790

### 791 **Image quantification**

792 To quantify the effect of the nanobodies on HKU1 infection of epithelia, the fluorescence  
793 intensity of spike positive pixels of 5 fields (160  $\mu$ m<sup>2</sup> each) spread over the surface of the sample  
794 was measured using ImageJ-Fiji.

795

### 796 **CRISPR-Cas9 knock-out**

797 crRNAs TMPRSS2 (CGGATGCACCTCGTAGACAG) and pre-designed unspecific  
798 crRNA used as control were ordered from Integrated DNA Technologies, IDT. crRNA and  
799 tracrRNA were resuspended in IDT Duplex Buffer according to the manufacturer's instructions.  
800 On the day of the nucleofection, duplexes were formed by mixing equimolar concentration of  
801 crRNA and tracrRNA, followed by 5-min annealing at 95°C. 100 pmol of RNA duplexes were  
802 then mixed (1:2) with 50 pmol TrueCut™ Cas9 Protein v2 (Thermo Fisher Scientific) for 10  
803 min at RT to generate ribonucleoprotein (RNP) complexes. Caco2 were resuspended in SE cell  
804 line buffer Solution (Lonza), mixed with RNP and Alt-R® Cas9 Electroporation Enhancer (90  
805 pmol, IDT), and nucleofected in a 4D-Nucleofector™ System (Lonza) using the SE Cell line  
806 4D-Nucleofector™ X Kit S (program DG-113). After nucleofection, cells were seeded in  
807 DMEM 10% FBS. 48 h post transfection, cells were subcloned. Clones were screened for  
808 TMPRSS2 knock-out by staining using VHH-A01-Fc and flow cytometry (immunostaining  
809 section). Knock out was confirmed by PCR and sequencing the target region using the

810 following primers: forward (5'-AAGACGGAGGAGAAGGGTCA-3') and reverse (5'-  
811 AGTTGTAGACACCTAGGGAGAA-3').

812

### 813 **Protein production**

#### 814 *Construct design*

815 Spike, RBD, TMPRSS2 and ACE2 constructs were obtained from Genscript as codon-  
816 optimized synthetic genes. Ectodomains from HKU1A (residues 14-1281) and B (residues 14-  
817 1276) were cloned into pcDNA3.1(+), downstream of a murine Ig kappa signal peptide  
818 (METDTLLLWVLLLWVPGSTG) and upstream of a thrombin cleavage site followed by a  
819 His-tag. Spikes were stabilized by mutating the furin cleavage site (<sup>756</sup>RRKRR<sup>760</sup>><sup>756</sup>GGSGS<sup>760</sup>  
820 in HKU1A; <sup>752</sup>RRKRR<sup>756</sup>><sup>752</sup>GGSGS<sup>756</sup> in HKU1B;), two residues in the S2 subunit  
821 (<sup>1071</sup>AL<sup>1072</sup>><sup>1071</sup>PP<sup>1072</sup> in HKU1A; <sup>1067</sup>NL<sup>1068</sup>><sup>1067</sup>PP<sup>1068</sup> in HKU1B) and adding a Foldon  
822 trimerization motif at the C-terminus. The ectodomain from the Wuhan SARS-CoV-2 Spike  
823 (residues 1-1208) was cloned into pcDNA3.1(+) and was stabilized with 6 proline mutations  
824 (F817P, A892P, A899P, A942P, K986P, V987P), as reported<sup>64</sup>. The furin site was also replaced  
825 as above (<sup>682</sup>RRAR<sup>685</sup>><sup>682</sup>GSAS<sup>685</sup>), a C-terminal Foldon motif was introduced, as well as  
826 Hisx8, Strep, and Avi tags.

827 The RBDs (residues 323-609 for HKU1A; 323-607 for HKU1B; 331-528 for SARS-CoV-2  
828 Wuhan) were cloned into pCAGGS (HKU1) or pcDNA3.1(+) (SARS-CoV-2), following a  
829 murine immunoglobulin kappa signal peptide, and upstream of a thrombin cleavage site and *in-*  
830 *tandem* Hisx8, Strep and Avi-tags. The WT TMPRSS2 ectodomain (residues 107-492)  
831 followed by C-terminal tags (8xHis-tag and AviTag) was synthesized and cloned into  
832 pcDNA3.1/Zeo(+) expression vector (Thermo Fisher Scientific). The TMPRSS2 ectodomain  
833 with the S441A mutation was cloned into a modified pMT/BiP plasmid (Invitrogen; hereafter  
834 termed pT350), which translates the protein in frame with an enterokinase cleavage site and a  
835 double strep-tag at the C-terminal end. The ACE2 peptidase domain (residues 19-615) was  
836 cloned in pcDNA3.1(+) with a murine immunoglobulin kappa signal peptide and a C-terminal  
837 thrombin cleavage site followed by a Strep-tag. The coding sequences of the selected VHHs in  
838 the vector pHEN6 were subcloned into a bacterial expression vector pET23 encoding a C  
839 terminal His-tag using NcoI and NotI restriction sites.

840

#### 841 *Protein expression and purification*

842 RBD, spike and ACE2-encoding plasmids were transiently transfected into Expi293F<sup>TM</sup>  
843 cells (Thermo-Fischer) using FectoPro DNA transfection reagent (PolyPlus) or

844 polyethylenimine (PEI) precipitation method, as previously described<sup>65</sup>. After 5 days at 37 °C,  
845 cells were harvested by centrifugation and the supernatants were concentrated. The spike  
846 proteins used for flow cytometry were purified from culture supernatants by high-performance  
847 chromatography using the Ni Sepharose Excel Resin according to the manufacturer's  
848 instructions (GE Healthcare) and dialyzed against PBS using Slide-A-Lyzer dialysis cassettes  
849 (Thermo Fisher Scientific). The spike proteins used for ELISA were further purified by size-  
850 exclusion chromatography (SEC) on a Superose6 10/300 column (Cytiva). Eluted fractions  
851 were analyzed by SDS-PAGE and those containing bands of the expected molecular weight  
852 were pooled, concentrated and further purified by SEC on a Superdex 200 10/300 column  
853 (Cytiva). AviTagged SARS-CoV-2 tri-S used for flow cytometry was biotinylated using  
854 Enzymatic Protein Biotinylation Kit (Sigma-Aldrich). HKU1A and HKU1B spike proteins  
855 used for ELISA were biotinylated using EZ-Link™ Sulfo-NHS-biotinylation kit (Thermo  
856 Fisher Scientific). The HKU1B RBD used for the BLI experiment with nanobodies was  
857 biotinylated with the BirA biotin-protein ligase standard reaction kit (Avidity).

858 The pT350 plasmid encoding S441A TMPRSS2 was used to perform a stable transfection  
859 on *Drosophila* S2 cells with the pCoPuro plasmid for puromycin selection. The cell line was  
860 selected and maintained in serum-free insect cell medium (HyClone, GE Healthcare) containing  
861 7 µg/mL puromycin and 1% penicillin/streptomycin. For protein production, the cells were  
862 grown in spinner flasks until the density reached 10<sup>7</sup> cells/mL, at which point the protein  
863 expression was induced with 4 µM CdCl<sub>2</sub>. After 6 days, the culture was centrifuged and the  
864 supernatant was concentrated and used for affinity purification using a Streptactin column  
865 (IBA). The eluate was concentrated and applied onto a Superdex 200 16/60 column (Cytiva)  
866 equilibrated with 10 mM Tris-HCl (pH 8.0), 100 mM NaCl.

867 *E. coli* BL21pLysS cells were transformed with the plasmids encoding the different VHHs,  
868 which were expressed in the cytoplasm after overnight induction with 0.5 mM IPTG at 16°C.  
869 The cultures were centrifuged, the bacterial pellets were resuspended in 40 mL of lysis buffer  
870 (20 mM Tris-HCl, 200 mM NaCl, 20 mM imidazole, pH 8.0) containing complete protease  
871 inhibitor cocktail (Roche) and they were frozen at -80°C until used. On the purification day,  
872 the resuspended pellets were thawed, sonicated (15 min, 9s on-pulse, 5s off-pulse), centrifuged  
873 and loaded onto a HisTrap column. Bound proteins were eluted with a linear gradient of buffer  
874 B (20 mM Tris-HCl, 200 mM NaCl, 500 mM imidazole, pH 8.0) and analyzed by SDS-PAGE.  
875 Fractions with higher purity were pooled, concentrated and further purified by SEC on a

876 Superdex 75 16/60 column (Cytiva) pre-equilibrated in 10 mM Tris-HCl, 100 mM NaCl, pH  
877 8.0.

878 The purity of the final protein samples was analyzed by SDS-PAGE followed by Coomassie  
879 Blue staining or silver staining. For gels, see SI 2.

880

### 881 **Flow cytometry**

882 For Spike binding, 293T cells were transiently transfected with TMPRSS2 and maintained  
883 in the presence or absence of Camostat (10  $\mu$ M) for 24 h. The cells were incubated with soluble  
884 biotinylated spike diluted in MACS buffer (PBS, 5 g/L BSA, 2 mM EDTA) at 2  $\mu$ g/mL for  
885 30 min at 4°C. The cells were then washed twice with PBS and then incubated with Alexa Fluor  
886 647-conjugated streptavidin (Thermo Fisher Scientific, S21374, 1:400) for 30 min at 4°C. The  
887 cells were washed once with PBS and fixed with 4% paraformaldehyde. The results were  
888 acquired using an Attune Nxt Flow Cytometer (Life Technologies, software v3.2.1).  
889 Transfection efficiency for TMPRSS2 was assessed by using either a commercial anti-  
890 TMPRSS2 antibody (for the experiments performed at the initiation of the study), the anti-  
891 TMPRSS2 monomeric VHH or the dimeric VHH A01-Fc (see below).

892 The staining with the commercial anti-TMPRSS2 antibody was performed on fixed cells by  
893 staining intracellularly with rabbit anti-TMPRSS2 (Atlas HPA035787), for 30 min at RT in  
894 PBS/BSA/Azide/0.05% Saponin followed by a Alexa Fluor 647 Goat anti-Rabbit antibody  
895 (Thermo Fisher Scientific, A-21245, 1:500).

896 For the spike, transfection efficiency was measured at the surface of live cells using mAb10  
897 diluted in MACS buffer for 30 min at 4°C, and a human secondary IgG. mAb10 is an antibody  
898 generated from a SARS-CoV-2 infected patient which cross-reacts with HKU1<sup>30</sup>.

899 Surface expression of TMPRSS2 was assessed on live cells by staining with anti-TMPRSS2  
900 VHH-A01-Fc (described in the study) at 1  $\mu$ g/mL, for 30 min at 4°C in MACS buffer, followed  
901 by staining with Alexa Fluor 647-conjugated Goat anti-Human antibody (Thermo Fisher  
902 Scientific, A-21445, 1:500). The control VHH Fc ctrl (R3VQFc) recognizes an unrelated  
903 protein (phosphorylated Tau protein)<sup>62</sup>.

904 The monomeric VHHs were used at 0.5  $\mu$ g/mL in MACS buffer for 30 min at 4°C, staining  
905 was revealed using a coupled anti-His antibody (R&D Systems, IC0501R, 1:1000).

906 Transfection efficiency for myc-tagged constructs was assessed on fixed cells by staining  
907 intracellularly with mouse anti-c-myc antibody, clone 9E10 (Thermo - M4439), for 30 min at  
908 RT in PBS/BSA/Azide/0.05% Saponin followed by an Alexa Fluor 647-conjugated Goat anti-  
909 Mouse antibody (Thermo Fisher Scientific, A-21242, 1:500). Transfection efficiency of APN

910 (CD13) and DPP4 (CD26) was assessed on live cells by surface staining in MACS buffer with  
911 CD13-PE (130-120-312, Miltenyi Biotec, 1:50) and CD26-PE (130-126-41, Miltenyi Biotec,  
912 1:50) for 30 min at 4°C. The cells were washed twice with PBS and fixed with 4%  
913 paraformaldehyde. The results were acquired using an Attune Nxt Flow Cytometer (Life  
914 Technologies). Gating strategies are described in SI 3.

915

#### 916 **Sialic acid staining**

917 Cells were harvested using PBS/0.1% EDTA for 5 min at 37°C, washed in PBS and stained  
918 1 h at 4°C in PBS/1% SVF containing either 10 µg/mL Sambucus Nigra Lectin-FITC (Lectin  
919 NSA) (L32479 – Thermo) or 2.5 µg/mL recombinant mouse Siglec E-Fc (551504 –  
920 BioLegend). Cells were washed twice in PBS. Lectin-stained cells were fixed for 10 min in 4%  
921 paraformaldehyde. Siglec-E-Fc stained cells were further incubated with Alexa Fluor 647-  
922 conjugated Goat anti-Human antibody (Thermo Fisher Scientific, A-21445, 1:500) for 30 min  
923 at 4°C before being fixed for 10 min in 4% paraformaldehyde.

924

#### 925 **ELISA assay**

926 ELISAs were performed as previously described<sup>66</sup>. Briefly, high-binding 96-well ELISA  
927 plates (Costar; Corning) were coated overnight with 250 ng/well of purified TMPRSS2 or  
928 ACE2. After washing with 0.05% Tween 20-PBS (washing buffer), the plates were blocked for  
929 2 h with 2% BSA, 1 mM EDTA, 0.05% Tween 20-PBS (Blocking buffer), washed, and  
930 incubated with serially diluted soluble biotinylated spike proteins. Recombinant spike proteins  
931 were tested at 100 µg/mL, and at 7 consecutive 1:2 dilutions in PBS. After washings, the plates  
932 were revealed by incubation for 1 h with HRP-conjugated streptavidin (BD Biosciences) in  
933 blocking buffer and by adding 100 µL of HRP chromogenic substrate (ABTS solution,  
934 Euromedex) after washing steps. Optical densities were measured at 405 nm (OD<sub>405nm</sub>) and  
935 background values given by incubation of PBS alone in coated wells were subtracted.  
936 Experiments were performed using HydroSpeed microplate washer and Sunrise microplate  
937 absorbance reader (Tecan).

938

#### 939 **BLI assay**

940 Affinity of recombinant RBDs towards the purified ectodomains of S441A TMPRSS2 or  
941 ACE2 was assessed in real-time using a bio-layer interferometry Octet-Red384 device (Pall  
942 ForteBio). Nickel-NTA capture sensors (Sartorius) were loaded for 10 min at 1000 rpm shaking  
943 speed with the Wuhan RBD at 100 nM or the HKU1A/B RBDs at 200 nM in PBS. The sensors

944 were then blocked with PBS containing BSA at 0.2 mg/mL (assay buffer) and were incubated  
945 at 1000 rpm with two-fold serially diluted concentrations (800 nM to 3.12 nM) of S441A  
946 TMPRSS2 or ACE2 ectodomains in assay buffer. Association and dissociation were monitored  
947 for 300 s and 240 s, respectively. Measurements for a reference sensor were recorded using a  
948 sensor loaded with an unrelated protein (CD147) that was dipped at each analyte concentration.  
949 A sample reference measurement was recorded from a sensor loaded with either RBD and  
950 dipped in the assay buffer. Specific signals were calculated by double referencing, subtracting  
951 nonspecific signals obtained for the sensor and sample references from the signals recorded for  
952 the RBD-loaded sensors dipped in S441A TMPRSS2 solutions. The steady-state signal was  
953 plotted against the analyte concentration and the curve was fitted assuming a 1:1 binding model.

954 The affinity of the nanobodies for the S441A TMPRSS2 ectodomain was determined using  
955 a similar procedure. Nickel-NTA capture sensors were loaded with each nanobody at 100 nM  
956 in PBS, then blocked with assay buffer and incubated at 1000 rpm with two-fold serially diluted  
957 concentrations (400 nM to 3.12 nM) of S441A TMPRSS2. Association and dissociation were  
958 monitored for 240 s and 180 s, respectively. A sample reference measurement was recorded  
959 from a sensor loaded with each nanobody and dipped in the assay buffer. Association and  
960 dissociation profiles were fitted assuming a 1:1 binding model.

961 Experiments to identify anti-TMPRSS2 nanobodies that block binding to the HKU1 RBD  
962 were performed by immobilizing the biotinylated HKU1B RBD on Streptavidin capture  
963 sensors. They were blocked in assay buffer and dipped into solutions containing a pre-incubated  
964 mixture of TMPRSS2 S441A (200 nM) and a nanobody (400 nM). The signal corresponding  
965 to the association was recorded.

966

#### 967 **TMPRSS2 enzymatic activity**

968 Enzymatic activity was measured using BOC-QAR-AMC (R&D Systems, ES014), a  
969 substrate of TMPRSS2 that fluoresces when cleaved. For wild type and mutant TMPRSS2,  
970 cells were transfected in a black bottom 96 well plate as described above. After 24 h, media  
971 was replaced with 100  $\mu$ L FCS free, phenol red free media, containing 100  $\mu$ M of fluorogenic  
972 substrate. Indicated concentration of inhibitors were added. When the assay was performed  
973 with soluble TMPRSS2, 60 nM of soluble protein was added to the well and mixed with VHH  
974 nanobodies for 15 min, before adding 100  $\mu$ M of fluorogenic substrate.

975

#### 976 **Western Blot**

977 Cells were lysed in TXNE buffer (1% Triton X-100, 50 mM Tris-HCl (pH 7.4), 150 mM  
978 NaCl, 5 mM EDTA, 1X Roche cOmplete protease inhibitors) for 30 min on ice. Equal amounts  
979 (10 µg) of cell lysates were analyzed by Western blot. The following antibodies were diluted  
980 in WB buffer (PBS, 1% BSA, 0.05% Tween, 0.01% Na Azide): rabbit anti-human TMPRSS2  
981 (Atlas antibodies cat# HPA035787, 1:1,000), mouse anti-beta actin (Abcam, 60008-1-Ig,  
982 1:2,000), rabbit anti-HKU1 S1 polyclonal antibody (Thermofisher Scientific Cat #PA5-120768,  
983 1:2,000) and rabbit anti-HKU1 S2 polyclonal antibody (Thermofischer Scientific #PA5-  
984 120769, 1:1,000). Species-specific secondary DyLight-coupled antibodies were used  
985 (1:10,000) and proteins were revealed using a Licor Imager. Images were processed using  
986 Image Studio Lite software v5.2.5.

987

## 988 **Nanobody isolation and production**

### 989 **Alpaca immunization**

990 Animal procedures were performed according to the French legislation and in compliance  
991 with the European Communities Council Directives (2010/63/UE, French Law 2013-118,  
992 February 6, 2013). The Animal Experimentation Ethics Committee of Pasteur Institute  
993 (CETEA 89) approved this study (2020-27412). One young adult male alpaca (*Lama pacos*)  
994 was immunized at days 0, 17, and 24 with 150 µg of S4441A TMPRSS2. The immunogen was  
995 mixed with Freund complete adjuvant for the first immunization and with Freund incomplete  
996 adjuvant for the following immunizations. The immune response was monitored by titration of  
997 serum samples by ELISA on coated TMPRSS2. The bound alpaca antibodies were detected  
998 with polyclonal rabbit anti-alpaca IgGs<sup>67</sup>.

999

### 1000 **Library construction and phage display**

1001 The blood of the immunized animal (about 300 mL) was collected and peripheral blood  
1002 lymphocytes were isolated by centrifugation on a Ficoll (Cytiva, Velizy, France) discontinuous  
1003 gradient and stored at -80°C until further use. Total RNA and cDNA were obtained as  
1004 previously described<sup>67</sup>. The VHH repertoires were amplified from the cDNA by two successive  
1005 PCR reactions and the VHH fragments were cloned into the SfiI/NotI restriction sites of pHEN6  
1006 phagemid vector<sup>62</sup>. The selection of specific phage-VHHs was performed by phage display. A  
1007 large number of phage-VHHs (10<sup>13</sup>) was used to perform 3 rounds of panning. Briefly, Phage-  
1008 VHHs were incubated for 1 h with TMPRSS2 that has been previously coated on an  
1009 immunotube (Nunc). To remove non-specific binders, an extensive washing procedure was  
1010 performed and specific phage-VHHs were eluted in 100 mM triethylamine (TEA). *E.coli* TG1

1011 at exponential growth phase were then infected with eluted phage-VHHs. Phage-VHHs were  
1012 produced from individual colonies and binding of the phages to TMPRSS2 on plate was  
1013 revealed with an anti-M13 monoclonal antibody conjugated to peroxidase (Abcam). The VHH  
1014 nucleotide sequences were determined using M13-40 primer (Eurofins, Ebersberg, Germany).

1015

#### 1016 **Production of VHHs**

1017 The coding sequences of the selected VHHs in the vector pHEN6 were subcloned into a  
1018 bacterial expression vector pET23 encoding a C terminal His tag using NcoI and NotI  
1019 restriction sites. Sequences of the VHH are available in SI 4. Transformed *E. coli* BL21pLysS  
1020 cells expressed VHHs in the cytoplasm after overnight induction with 0.5 mM IPTG at 16°C.  
1021 Purified VHHs were isolated on Co<sup>++</sup> affinity columns from cytoplasmic extracts treated by  
1022 10 U/mL Benzonase Nuclease (Merck) and Complete protease inhibitor (Roche), according to  
1023 the manufacturer's instructions, followed by size exclusion chromatography (SEC) with a  
1024 Superdex 75 column (Cytiva).

1025

#### 1026 **Production of dimeric VHH-Fc**

1027 VHHs' engineered genes were cloned into a pFUSE-derived vector (InvivoGen); this vector  
1028 harbors a human IgG1-Fc domain. Consequently, the VHH was expressed as a Fc-fusion  
1029 bivalent antibody. The vector was used to transform Expi293F mammalian cells  
1030 (ThermoFisher), and protein expression was carried out according to manufacturer's  
1031 recommendations. Protein was purified from the expression medium by affinity  
1032 chromatography on a 1 mL protein G column (Cytiva). After sample application, the column  
1033 was washed with 20 column volumes of PBS and the protein was subsequently eluted with 10  
1034 column volumes of PBS supplemented with 0.1 M Glycine (pH=2.3). Affinity-eluted VHH-Fc  
1035 were finally polished on a HiLoad 16/600 Superdex 200pg Pre-packed column (Cytiva) using  
1036 PBS buffer<sup>68</sup>

1037

#### 1038 **Statistical analysis**

1039 Flow cytometry data were analyzed with FlowJo<sup>TM</sup> v10.8 software (BD Life Science).  
1040 Calculations were all performed with Microsoft Excel 365. GraphPad Prism 9 for Mac was  
1041 used to generate figures and for statistical analysis (GraphPad Software). Statistical significance  
1042 between different conditions was calculated using the tests indicated in the corresponding figure  
1043 legends.

1044

1045 **Illustrations**

1046 All illustrations were generated by using Inkscape. They can be re-used if cited properly.

1047 **Additional references**

- 1048 47 Kodaka, M. *et al.* A new cell-based assay to evaluate myogenesis in mouse myoblast  
1049 C2C12 cells. *Exp. Cell Res.* **336**, 171-181 (2015).  
1050 [https://doi.org:https://doi.org/10.1016/j.yexcr.2015.06.015](https://doi.org/https://doi.org/10.1016/j.yexcr.2015.06.015)
- 1051 48 Edie, S. *et al.* Survey of Human Chromosome 21 Gene Expression Effects on Early  
1052 Development in *Danio rerio*. *G3: Genes, Genomes, Genetics* **8**, 2215-2223 (2018).  
1053 <https://doi.org:10.1534/g3.118.200144>
- 1054 49 Hayer, A. *et al.* Engulfed cadherin fingers are polarized junctional structures between  
1055 collectively migrating endothelial cells. *Nat. Cell Biol.* **18**, 1311-1323 (2016).  
1056 <https://doi.org:10.1038/ncb3438>
- 1057 50 Rajah, M. M. *et al.* SARS-CoV-2 Alpha, Beta, and Delta variants display enhanced  
1058 Spike-mediated syncytia formation. *The EMBO Journal* **n/a**, e108944 (2021).  
1059 <https://doi.org:https://doi.org/10.15252/embj.2021108944>
- 1060 51 Iglesias, M. C. *et al.* Lentiviral vectors encoding HIV-1 polyepitopes induce broad  
1061 CTL responses in vivo. *Mol. Ther.* **15**, 1203-1210 (2007).  
1062 <https://doi.org:10.1038/sj.mt.6300135>
- 1063 52 Loens, K. *et al.* Performance of Different Mono- and Multiplex Nucleic Acid  
1064 Amplification Tests on a Multipathogen External Quality Assessment Panel. *J. Clin.*  
1065 *Microbiol.* **50**, 977-987 (2012). <https://doi.org:doi:10.1128/jcm.00200-11>
- 1066 53 Matranga, C. B. *et al.* Enhanced methods for unbiased deep sequencing of Lassa and  
1067 Ebola RNA viruses from clinical and biological samples. *Genome Biol* **15**, 519 (2014).  
1068 <https://doi.org:10.1186/preaccept-1698056557139770>
- 1069 54 Bolger, A. M., Lohse, M. & Usadel, B. Trimmomatic: a flexible trimmer for Illumina  
1070 sequence data. *Bioinformatics* **30**, 2114-2120 (2014).  
1071 <https://doi.org:10.1093/bioinformatics/btu170>
- 1072 55 Li, D. *et al.* MEGAHIT v1.0: A fast and scalable metagenome assembler driven by  
1073 advanced methodologies and community practices. *Methods* **102**, 3-11 (2016).  
1074 <https://doi.org:https://doi.org/10.1016/j.ymeth.2016.02.020>
- 1075 56 Buchfink, B., Xie, C. & Huson, D. H. Fast and sensitive protein alignment using  
1076 DIAMOND. *Nat. Methods* **12**, 59-60 (2015). <https://doi.org:10.1038/nmeth.3176>
- 1077 57 Katoh, K. & Standley, D. M. MAFFT Multiple Sequence Alignment Software Version  
1078 7: Improvements in Performance and Usability. *Mol. Biol. Evol.* **30**, 772-780 (2013).  
1079 <https://doi.org:10.1093/molbev/mst010>
- 1080 58 Martin, D. P., Murrell, B., Khoosal, A. & Muhire, B. in *Bioinformatics: Volume I:*  
1081 *Data, Sequence Analysis, and Evolution* (ed Jonathan M. Keith) 433-460 (Springer  
1082 New York, 2017).
- 1083 59 Kalyaanamoorthy, S., Minh, B. Q., Wong, T. K. F., von Haeseler, A. & Jermin, L. S.  
1084 ModelFinder: fast model selection for accurate phylogenetic estimates. *Nat. Methods*  
1085 **14**, 587-589 (2017). <https://doi.org:10.1038/nmeth.4285>
- 1086 60 Hoang, D. T., Chernomor, O., von Haeseler, A., Minh, B. Q. & Vinh, L. S. UFBoot2:  
1087 Improving the Ultrafast Bootstrap Approximation. *Mol. Biol. Evol.* **35**, 518-522  
1088 (2017). <https://doi.org:10.1093/molbev/msx281>
- 1089 61 Hadfield, J. *et al.* Nextstrain: real-time tracking of pathogen evolution. *Bioinformatics*  
1090 **34**, 4121-4123 (2018). <https://doi.org:10.1093/bioinformatics/bty407>

- 1091 62 Gransagne, M. *et al.* Development of a highly specific and sensitive VHH-based  
1092 sandwich immunoassay for the detection of the SARS-CoV-2 nucleoprotein. *J. Biol.*  
1093 *Chem.* **298**, 101290 (2022). <https://doi.org/10.1016/j.jbc.2021.101290>  
1094 63 Robinot, R. *et al.* SARS-CoV-2 infection induces the dedifferentiation of multiciliated  
1095 cells and impairs mucociliary clearance. *Nature Communications* **12**, 4354 (2021).  
1096 <https://doi.org/10.1038/s41467-021-24521-x>  
1097 64 Hsieh, C.-L. *et al.* Structure-based design of prefusion-stabilized SARS-CoV-2 spikes.  
1098 *Science* **369**, 1501-1505 (2020). <https://doi.org/doi:10.1126/science.abd0826>  
1099 65 Lorin, V. & Mouquet, H. Efficient generation of human IgA monoclonal antibodies. *J.*  
1100 *Immunol. Methods* **422**, 102-110 (2015).  
1101 <https://doi.org/https://doi.org/10.1016/j.jim.2015.04.010>  
1102 66 Mouquet, H. *et al.* Memory B cell antibodies to HIV-1 gp140 cloned from individuals  
1103 infected with clade A and B viruses. *PLoS One* **6**, e24078 (2011).  
1104 <https://doi.org/10.1371/journal.pone.0024078>  
1105 67 Lafaye, P., Achour, I., England, P., Duyckaerts, C. & Rougeon, F. Single-domain  
1106 antibodies recognize selectively small oligomeric forms of amyloid beta, prevent  
1107 Abeta-induced neurotoxicity and inhibit fibril formation. *Mol. Immunol.* **46**, 695-704  
1108 (2009). <https://doi.org/10.1016/j.molimm.2008.09.008>  
1109 68 Li, Q. *et al.* Generation of nanobodies acting as silent and positive allosteric  
1110 modulators of the  $\alpha 7$  nicotinic acetylcholine receptor. *Cell. Mol. Life Sci.* **80**, 164  
1111 (2023). <https://doi.org/10.1007/s00018-023-04779-8>  
1112 69 Grubaugh, N. D. *et al.* An amplicon-based sequencing framework for accurately  
1113 measuring intrahost virus diversity using PrimalSeq and iVar. *Genome Biology* **20**, 8  
1114 (2019). <https://doi.org/10.1186/s13059-018-1618-7>  
1115  
1116  
1117

## 1118 Extended Data

1119  
1120  
1121 **Extended Data Figure 1. a. Binding of the 5 anti-TMPRSS2 VHH on recombinant**  
1122 **TMPRSS2 measured by BLI. b, c. Comparison of one commercial TMPRSS2 antibody**  
1123 **and of the dimeric anti-TMPRSS2 VHH A01-Fc.** 293T cells were transfected with WT  
1124 TMPRSS2. 24 h later, cells were analysed by flow-cytometry. Staining with the commercial  
1125 antibody was performed on fixed cells (**b**) while surface staining with the VHH was performed  
1126 on live cells (**c**).  
1127  
1128

1129 **Extended Data Figure 2. Effect of TMPRSS2 and other proteases on HKU1 cell-cell**  
1130 **fusion. a, b. Surface expression and fusogenic activity of HKU1 spikes. a.** 293T cells were  
1131 transfected with plasmids encoding for HKU1A or HKU1B spikes and stained 24 h later with  
1132 mAb10, a pan anti-coronavirus spike antibody. Data are representative of 3 independent  
1133 experiments. **b.** Cell-cell fusion mediated by HKU1A or HKU1B spikes. 293T GFP-Split cells  
1134 were transfected with HKU1 spikes and TMPRSS2, fusion was visualized by the appearance  
1135 of GFP<sup>+</sup> cells. Data are representative of 6 independent experiments. Scale bar: 400  $\mu$ m **c. Cell-**  
1136 **cell fusion mediated by the SARS-CoV-2 spike.** 293T GFP-Split cells were transfected with  
1137 SARS-CoV-2 spike, in the presence of ACE2 or TMPRSS2, fusion was visualized by the  
1138 appearance of GFP<sup>+</sup> cells. Data are mean  $\pm$  SD of 3 independent experiments **d. U2OS cell-**  
1139 **cell fusion mediated by HKU1A spike.** U2OS GFP-Split cells were transfected with HKU1A  
1140 spike and TMPRSS2, fusion was visualized by the appearance of GFP<sup>+</sup> cells 24 h later. Data

1141 are mean  $\pm$  SD of 3 independent experiments. **e. Expression levels of myc-tagged proteases.**  
1142 293T cells were transfected with a control plasmid or the indicated myc-tagged TMPRSS2  
1143 constructs and stained 24 h later with myc antibody 9E10. Left: Representative dot plots. Right:  
1144 Percentage of positive cells. Data are mean  $\pm$  SD of 3 independent experiments. **f. Surface**  
1145 **expression of tagged and untagged TMPRSS2.** 293T cells were transfected with WT  
1146 TMPRSS2 (TMPRSS2-Untagged) or a myc-tagged TMPRSS2 and surface stained for  
1147 TMPRSS2 using VHH-A01-Fc. Left: Representative dot plots. Right: Percentage of positive  
1148 cells. Data are mean  $\pm$  SD of 3 independent experiments. **g, h, i. Surface expression of APN,**  
1149 **DPP4 and ACE2.** 293T cells were transfected with APN, DPP4 or ACE2 plasmids, and surface  
1150 stained with the respective antibodies 24 h later. Left: Representative dot plots. Right:  
1151 Percentage of positive cells. Data are mean  $\pm$  SD of 3 (TMPRSS2, APN, DPP4) or 4 (ACE2)  
1152 independent experiments. **j. Images of time lapse microscopy of HKU1-mediated cell-cell**  
1153 **fusion** (extracted from Supp. video 1). 293T cells were transfected either with TMPRSS2-  
1154 scarlet-I or HKU1A S-NeonGreen. After 24 h, cells were mixed and imaged every 2.5 min for  
1155 2 h at 37°C.

1156  
1157 **Extended Data Figure 3. Knock-out and silencing of TMPRSS2 in Caco2 cells. a. Linear**  
1158 **diagram of the organization of the TMPRSS2 gene.** The CRISPR-Cas9 targeting site is  
1159 underlined and the proto-spacer recognition motif (PAM) is in bold. Rectangles represent  
1160 exons, black for 5' and 3' untranslated regions, gray for coding regions. **b. Sequence analysis**  
1161 **of the knock-out Caco2 clone.** Both alleles compared to the original wild-type sequence are  
1162 shown. The knockout clone harbors an out-of-frame deletion and an insertion, resulting in a  
1163 frameshift on both alleles. **c. Validation of TMPRSS2 knockout by TMPRSS2 surface**  
1164 **staining.** Representative dot plots of VHH anti-TMPRSS2 (VHH-A01-Fc) surface staining of  
1165 a WT and KO Caco2 obtained following CRISPR gene targeting. **d. Role of endogenous**  
1166 **TMPRSS2 on cell-cell fusion assessed by siRNA.** 293T donor cells expressing HKU1A spike  
1167 were mixed with Caco2 acceptor cells, silenced or not for TMPRSS2. Left: experimental  
1168 design. Middle: relative expression of TMPRSS2 in Caco2 cells, assessed by RT-qPCR. Data  
1169 were normalized to  $\beta$ -*Tubulin* levels. Relative mRNA expression normalized to siCtrl condition  
1170 ( $2^{-\Delta\Delta CT}$ ) was plotted. Right: fusion was quantified by measuring the GFP area after 20 h of  
1171 coculture. Data are mean  $\pm$  SD of 3 independent experiments. Statistical analysis: two-sided  
1172 unpaired t-test compared to siCtrl cells. \*\*\* $p < 0.0001$ .

1173  
1174 **Extended Data Figure 4. Effect of mutant TMPRSS2 on cell-cell fusion and pseudovirus**  
1175 **infection a. Enzymatic activity of WT and mutant TMPRSS2.** 293T cells were transfected  
1176 with WT and indicated TMPRSS2 mutants. 24 h post transfection, the catalytic activity was  
1177 assessed using BoC-QAR-AMC fluorogenic substrate. Data are mean  $\pm$  SD of 4 independent  
1178 experiments. Statistical analysis: a: one-way ANOVA with Dunnett's multiple comparisons  
1179 compared to Ctrl cells (transfected with pQCXIP-Empty). \*\* $p < 0.01$ . **b. Effect of TMPRSS2**  
1180 **on HKU1 spike expressed on adjacent cells.** 293T cells were transfected either with HKU1A  
1181 spike or with the different TMPRSS2. 20 h post-transfection, cells were mixed at a 1:1 ratio,  
1182 and let to settle. 3 or 6 h post-mixing, cells were harvested and lysed for WB. One membrane  
1183 was probed for S1, TMPRSS2 and actin, another membrane was probed for S2 and actin. For  
1184 gel source data, see SI 1c, d. Representative blots of 2. Molecular weights: kDa. The arrows  
1185 and # denote the uncleaved and cleaved protein products, respectively. **c. Surface levels of WT**  
1186 **and mutant TMPRSS2.** 293T cells were transfected with the indicated doses of TMPRSS2  
1187 plasmid. 18 h post-transfection they were stained intracellularly for TMPRSS2 using the  
1188 commercial antibody. Left: % of TMP positive cells. Right: Median fluorescent intensity  
1189 (MFI). #: indicates the chosen plasmid ratios to achieve similar TMPRSS2 levels with WT and

1190 indicated mutants. Data are mean  $\pm$  SD of 3 independent experiments. **d. Comparison of the**  
1191 **anti-TMPRSS2 commercial antibody and VHH staining in 293T cells.** 293T cells were  
1192 transfected with WT, R255Q and S441A TMPRSS2 plasmids. Cells were stained 24 h later  
1193 with the indicated antibodies and analysed by flow cytometry. One experiment representative  
1194 of 3 is shown. Light grey curves correspond to staining with control antibodies or VHH.  
1195 Parental: untransfected cells. **e. Effect of WT and mutant TMPRSS2 on SARS-CoV-2**  
1196 **pseudovirus infection.** 293T cells expressing ACE2 were transfected with WT and indicated  
1197 TMPRSS2 mutants. 24 h later, cells were infected by Luc-encoding SARS-CoV-2 pseudovirus.  
1198 Luminescence was measured after 48 h. Data are mean  $\pm$  SD of 4 independent experiments.  
1199 Statistical analysis: RM one-way ANOVA with Geisser-Greenhouse correction on log-  
1200 transformed data, with Dunnett's multiple comparisons compared to Ctrl cells (transfected with  
1201 pQCXIP-Empty). \*\* $p < 0.01$ . **f, g. Effect of SB412515, E64d or hydroxychloroquine (HCQ)**  
1202 **on f. HKU1A or g. HKU1B pseudovirus infection.** 293T cells expressing WT or S441A  
1203 TMPRSS2 were incubated for 2 h with the indicated drugs, before infection with HKU1A or  
1204 HKU1B pseudoviruses. Luminescence was read 48 h post infection. Left: SB412515. Middle:  
1205 E64d. Right: HCQ. Data are mean  $\pm$  SD of 3 (E64d, HKU1B), 4 (E64d HKU1A, SB142515  
1206 HKU1B), 5 (HCQ HKU1A) or 6 (HCQ HKU1B, SB412515 HKU1A) independent  
1207 experiments. Statistical analysis: RM two-way ANOVA with Geisser-Greenhouse correction on  
1208 non-normalized log transformed data, with Dunnett's multiple comparisons compared to the  
1209 non-treated conditions. **h, i. Surface levels of TMPRSS2 in different cell lines stably**  
1210 **expressing WT or S441 TMPRSS2.** Cells were stained for TMPRSS2 using VHH-A01-Fc  
1211 and analyzed by flow cytometry. Representative histograms are shown. **h.** Left: U2OS. Right:  
1212 A549. Light grey: cells stained with a non-target control VHH-Fc. Dark grey: Unmodified  
1213 parental cell lines. Dark and light blue: Cells transduced with either TMPRSS2 or TMPRSS2  
1214 S441A mutant. **i.** Caco2. Light grey: cells stained with a non-target control VHH-Fc. Blue:  
1215 Unmodified parental cell line. Dark Grey: TMPRSS2 KO Caco2. Dark and light blue:  
1216 TMPRSS2 KO caco2 stably transduced with TMPRSS2 WT or S441A mutant expression  
1217 vectors. **j. Effect of Camostat on endogenous TMPRSS2 in Caco2 cells.** Caco2 cells were  
1218 incubated in the presence of 100  $\mu$ M Camostat for 2 h, before infection with HKU1A, HKU1B,  
1219 or SARS-CoV-2 (D614G or Delta) pseudovirus. Data are normalized to the infection in the  
1220 absence of the drug. Data are mean  $\pm$  SD of 3 (SARS-CoV-2) or 4 (HKU1) independent  
1221 experiments. Statistical analysis: RM two-way ANOVA on non-normalized log transformed  
1222 data, with Sidak's multiple comparisons compared to the non-treated conditions. **k.**  
1223 **Susceptibility of Vero E6 and Vero E6-TMPRSS2 cells to HKU1 pseudovirus infection.**  
1224 Left: pseudovirus infection. Right: TMPRSS2 surface levels. Dark grey: Parental cells. Dark  
1225 blue: Cells transduced with TMPRSS2. Data are mean  $\pm$  SD of 4 independent experiments.

1226  
1227 **Extended Data Figure 5. Effect of neuraminidase on HKU1 pseudovirus infection.** U2OS-  
1228 TMPRSS2 cells were treated with indicated concentration of neuraminidase from *Arthrobacter*  
1229 *ureafaciens* for 24 h. **a. HKU1A and HKU1B pseudovirus infection in neuraminidase**  
1230 **treated cells.** Cells were infected with HKU1 A or B pseudoviruses. Luminescence was read  
1231 48 h post infection. Data were normalized to the non-treated condition. Data are mean  $\pm$  SD of  
1232 3 (4 mU/mL) or 4 (0, 20, 100 mU/mL) independent experiments. Statistical analysis: Mixed-  
1233 effect analysis with Geisser-Greenhouse corrections (handles missing values) on non-  
1234 normalized log transformed data, with Dunnett's multi-comparison test compared to non-  
1235 treated cells. **b. Surface levels of TMPRSS2 in neuraminidase treated cells.** Left: % of TMP  
1236 positive cells. Right: Median fluorescent intensity (MFI). Data are mean of 2 independent

1237 experiments. **c. Sambucus Nigra Lectin (SNA) binding on neuraminidase treated cells.**  
1238 Treated cells were stained with fluorescent Lectin SNA which preferentially binds  $\alpha$ -2,6- over  
1239  $\alpha$ -2,3 linked sialic acids. Left: Representative histograms. Right: MFI. Data are mean of 2  
1240 independent experiments. **d. Siglec-E binding on neuraminidase treated cells.** Treated cells  
1241 were stained with recombinant Siglec-E-Fc protein which preferentially binds  $\alpha$ 2,8- over  $\alpha$ 2,3-  
1242 and  $\alpha$ 2,6-linked sialic acids. Left: Representative histograms. Right: MFI. Data are mean  $\pm$  SD  
1243 of 3 independent experiments.  
1244

1245 **Extended Data Figure 6. Binding of HKU and SARS-CoV-2 spikes to TMPRSS2 or ACE2.**

1246 **a. Binding of the indicated recombinant spikes to 293T cells expressing TMPRSS2.** Cells  
1247 were transfected with WT or mutant TMPRSS2 and incubated or not overnight with 10  $\mu$ M of  
1248 Camostat. The spikes were then incubated for 0.5 h and their binding was revealed with  
1249 streptavidin-647 and measured by flow cytometry. The % of cells binding to TMPRSS2 was  
1250 quantified. Data are mean  $\pm$  SD of 3 (HKU1A) or 4 (HKU1B, SARS-CoV-2) independent  
1251 experiments. Two Way ANOVA with Dunnett's multiple comparisons compared to control  
1252 cells with or without Camostat. Exact p-values: HKU1A: TMPRSS2 WT-: \*0.029, TMPRSS2  
1253 WT+::\*\*\*<0.0001, TMPRSS2 R255Q-: \*\*0.0010, TMPRSS2 R255Q+: \*\*0,0013, TMPRSS2  
1254 S441A-: \*\*\*0,0001, TMPRSS2 S441A+: \*\*\*<0.0001. HKU1B: \*\*\*<0.0001. **b. Binding of**  
1255 **the indicated recombinant spikes to 293T cells expressing ACE2.** Cells were transfected  
1256 with ACE2. The spikes were then incubated for 0.5 h and their binding was revealed with  
1257 streptavidin-647 and measured by flow cytometry. The % of cells binding to ACE2 was  
1258 quantified. Data are mean of 2 independent experiments. **c. Binding of the indicated soluble**  
1259 **spikes on immobilized ACE2 measured by ELISA. d. Binding of S441A TMPRSS2 to**  
1260 **HKU1A, HKU1B or SARS-CoV-2 RBD measured by BLI.** The response was measured at  
1261 the indicated concentrations of spikes. Left: HKU1A. Middle: HKU1B. Right: SARS-CoV-2.  
1262 One representative experiment of 4 is shown. **e. Determination of the affinity of HKU1A and**  
1263 **B RBD for TMPRSS2 using the steady state method.** Circles: Experimental values. Black:  
1264 Fitting of the experimental data **f. Binding of ACE2 to SARS-CoV-2 or HKU1B RBD**  
1265 **quantified by BLI, at different concentrations of spikes. g. Binding of S441A TMPRSS2 to**  
1266 **HKU1B mutants.** Response was measured by BLI at different concentrations of spikes. Left:  
1267 HKU1B RBD mutant W515A. B: HKU1B RBD mutant R517A. **h. Determination of the**  
1268 **affinity of HKU1B-R517A RBD for TMPRSS2 using the steady state method.** Circles:  
1269 Experimental values. Black: Fitting of the experimental data. **i. Cell surface levels of WT and**  
1270 **mutant HKU1 spikes.** 293T were transfected with the indicated WT or mutant HKU1A or B  
1271 spikes, expression was measured by flow cytometry after 24 h, using the anti-spike mAb10.  
1272

1273 **Extended Data figure 7. Characterization of anti-TMPRSS2 VHHs. a. Binding of VHHs**

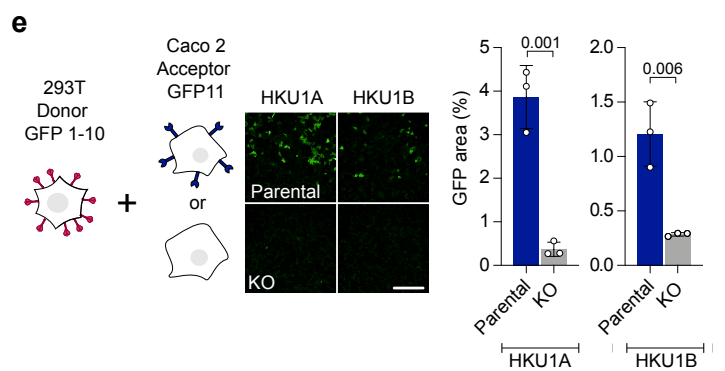
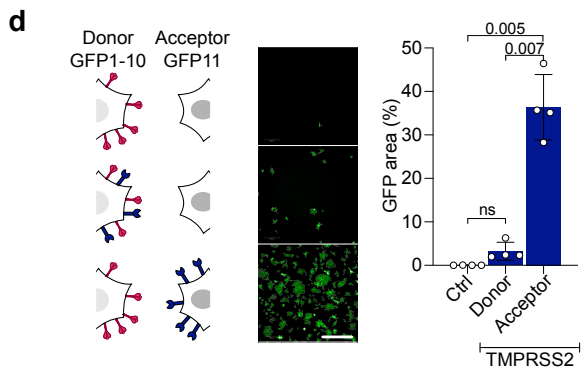
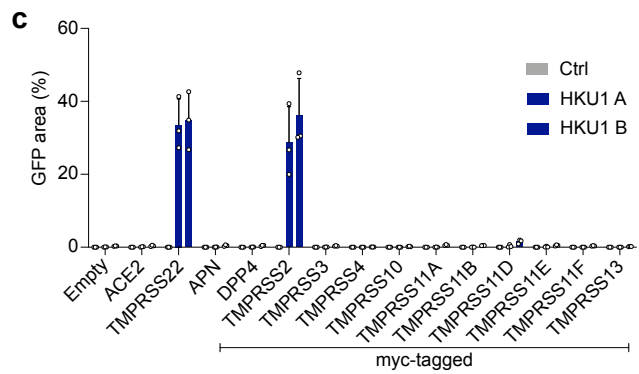
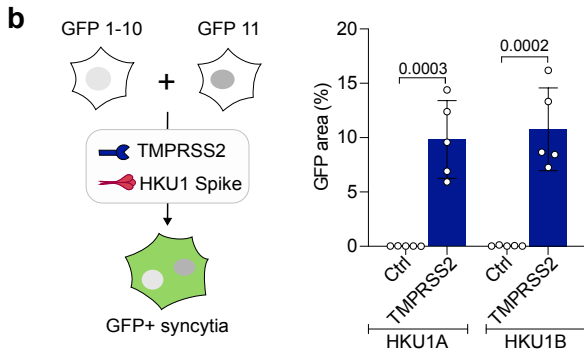
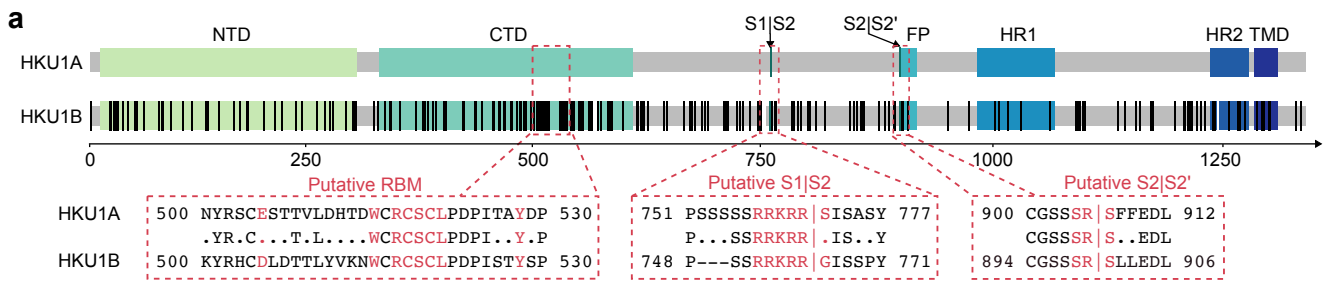
1274 **on TMPRSS2-expressing cells.** 293T cells were transfected with TMPRSS2 S441A. Binding  
1275 of the indicated VHHs (0.5  $\mu$ M) was assessed by flow cytometry. Left: representative dot plots.  
1276 Right: Quantification of the percentage of positive cells and MFI (Median Fluorescent Intensity  
1277 of positive cells). Data are mean  $\pm$  SD of three independent experiments **b. Effect of VHHs or**  
1278 **Camostat on TMPRSS2 enzymatic activity.** Recombinant soluble TMPRSS2 was incubated  
1279 with the indicated VHHs at different concentrations or with Camostat (1  $\mu$ M). The initial rate  
1280 of enzymatic activity, measured with a fluorescent substrate is plotted. One representative  
1281 experiment of 3 is shown. **c. Effect of VHHs on HKU1A or HKU1B cell-cell fusion.** 293T  
1282 GFP-Split cells were co-transfected with TMPRSS2 and HKU1 spike in the presence of  
1283 indicated amounts of VHH. Fusion was quantified by measuring the GFP area after 20 h. Data  
1284 were normalized to the non-treated condition for each spike. **d. Effect of VHHs on HKU1A**  
1285 **or HKU1B pseudovirus infection.** 293T cells transfected with S441A TMPRSS2 were  
1286 incubated with the indicated amounts of VHH for 2 h and infected by Luc-encoding

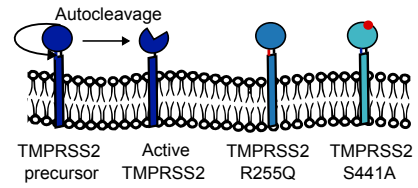
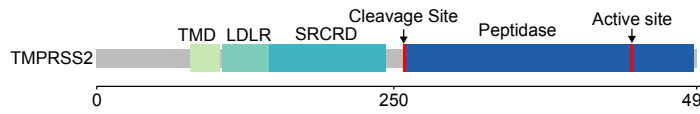
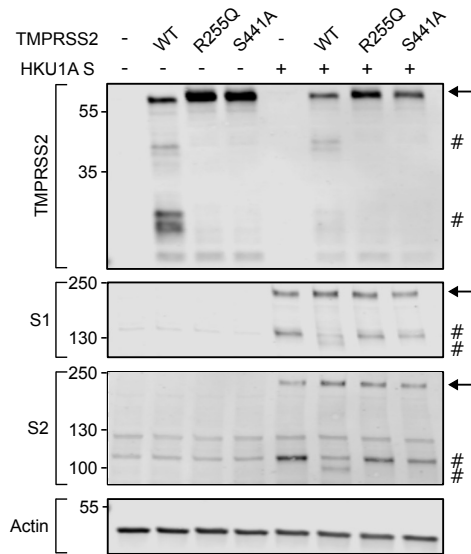
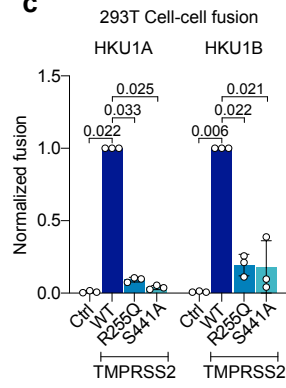
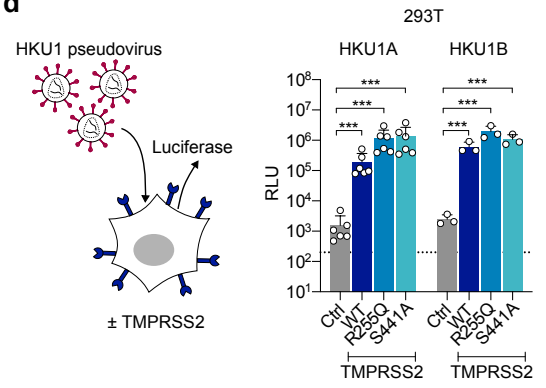
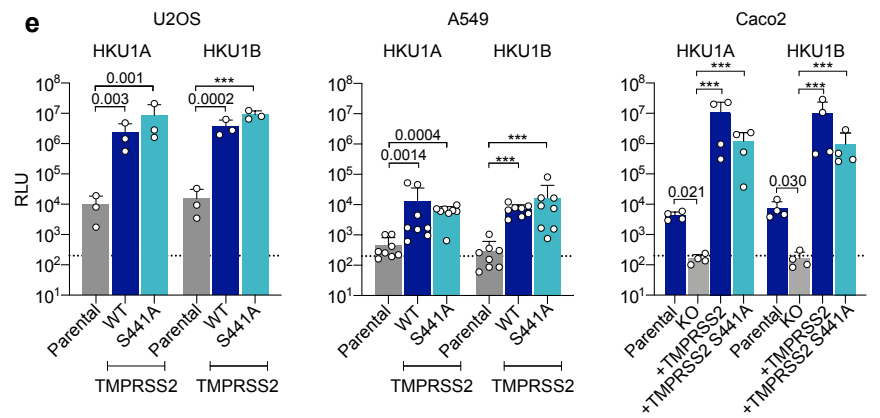
1287 pseudovirus. Luminescence was read 48 h post infection. Data were normalized to the non-  
1288 treated condition for each virus. Data are from one experiment representative of 3. **Statistical**  
1289 **analysis:** c: One Way ANOVA with Dunnett's multiple comparisons compared to cells stained  
1290 with a non-target antibody (VHH93). d: One Way ANOVA on log-transformed data with  
1291 Dunnett's multiple comparisons compared to cells stained with a non-target antibody (VHH93).

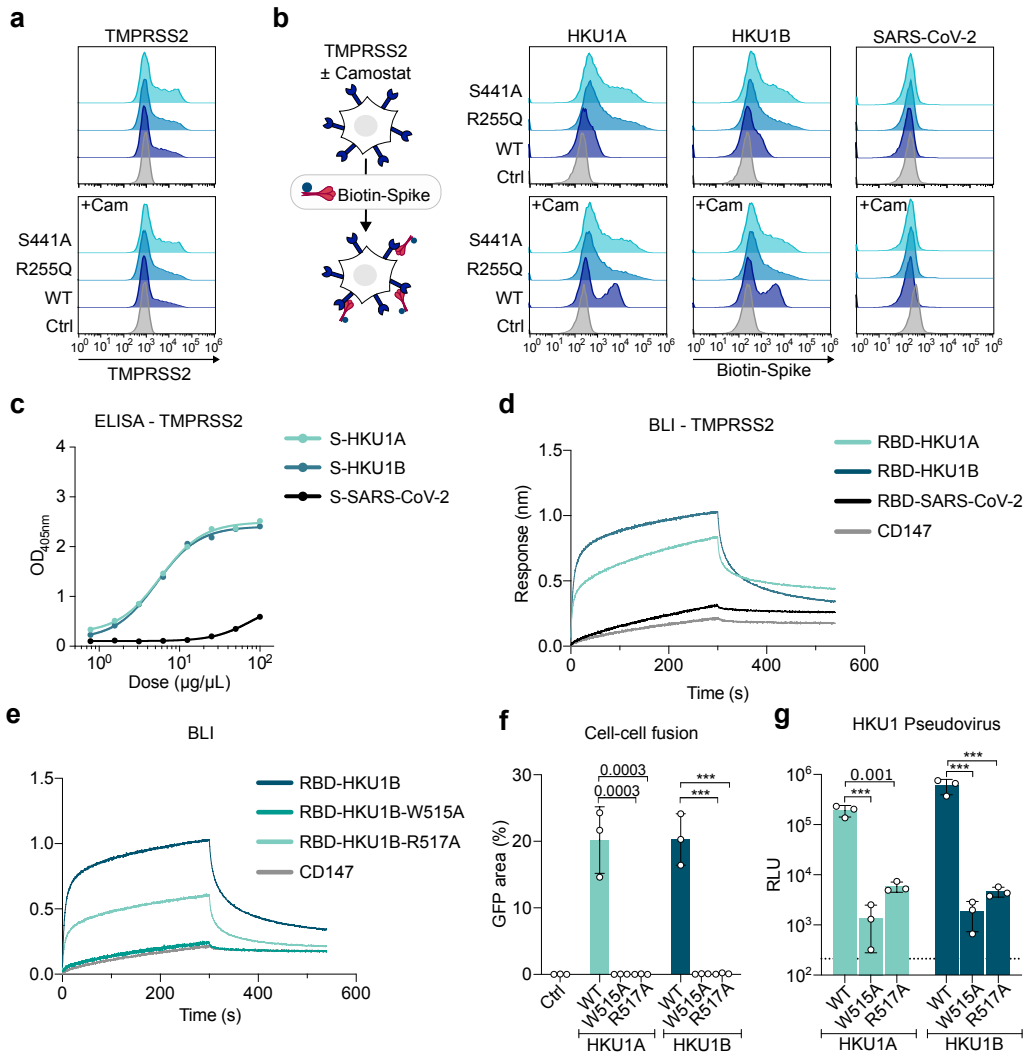
1292  
1293 **Extended data Figure 8. Isolation and characterization of a live HKU1B virus. a. Viral**  
1294 **RNA copies in the supernatant of HBE cells were quantified by RT-qPCR.** The values at  
1295 day 0 are the content of the input. Left: initial amplification (first passage). Right: Second  
1296 amplification of the first passage virus (harvested at day 4) used at two dilutions (1/10 and  
1297 1/100) in duplicates. **b. Reads coverage and frequency of minor variants frequencies of the**  
1298 **isolate sequencing data (first passage virus).** Intra-sample single-nucleotide variants  
1299 frequencies were estimated using iVAR<sup>69</sup>. The genome organization of HKU1 is shown below  
1300 the plot. **c, d. Phylogenetic analysis of HKU1.** Maximum likelihood phylogenies of human  
1301 coronavirus HKU1 (n = 48) estimated using IQ-TREE v2 with 1000 replicates from **c.** the  
1302 complete genome and **d.** spike coding sequences. The tree is midpoint rooted and ultrafast  
1303 bootstraps values are shown on the main branches. A similar topology was obtained when  
1304 rooting the tree using another embecovirus (OC43). The tip name corresponding to the newly  
1305 isolated virus sequence is highlighted in bold and underlined. The tips names corresponding to  
1306 the recombinant spikes used in this study are shown in bold.

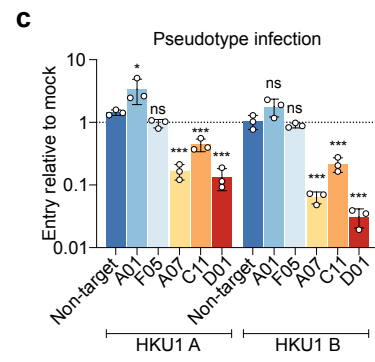
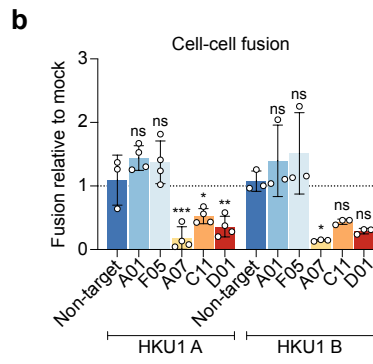
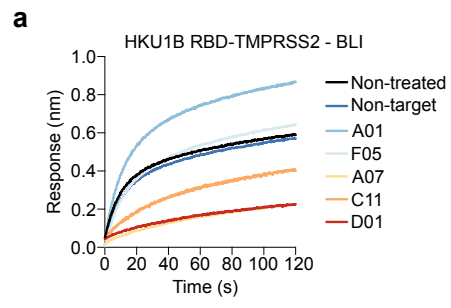
1307  
1308  
1309 **Extended data Table 1.** Affinity of the nanobodies for TMPRSS2 S441A and summary of  
1310 their effect.

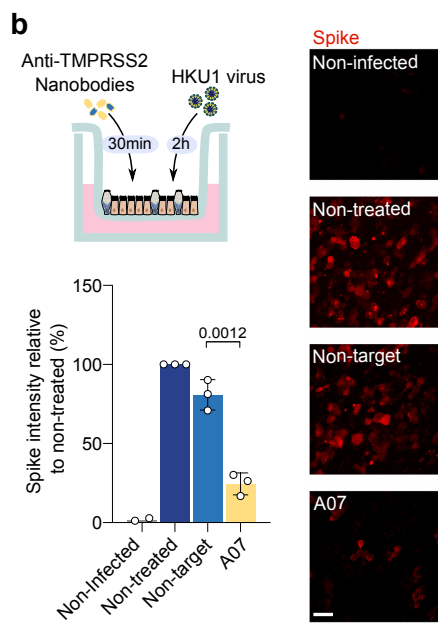
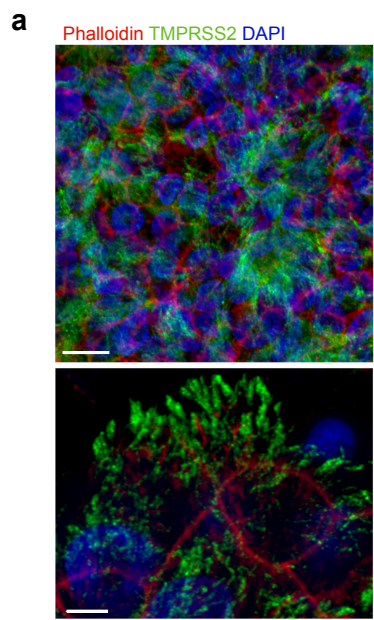
1311



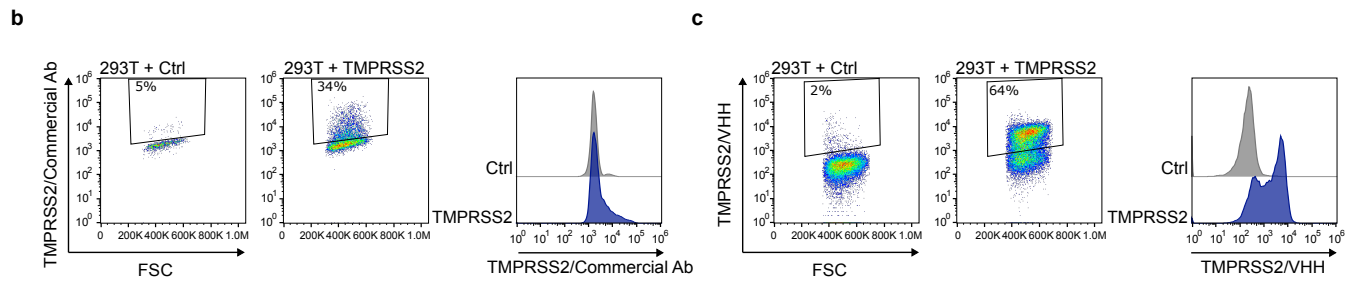
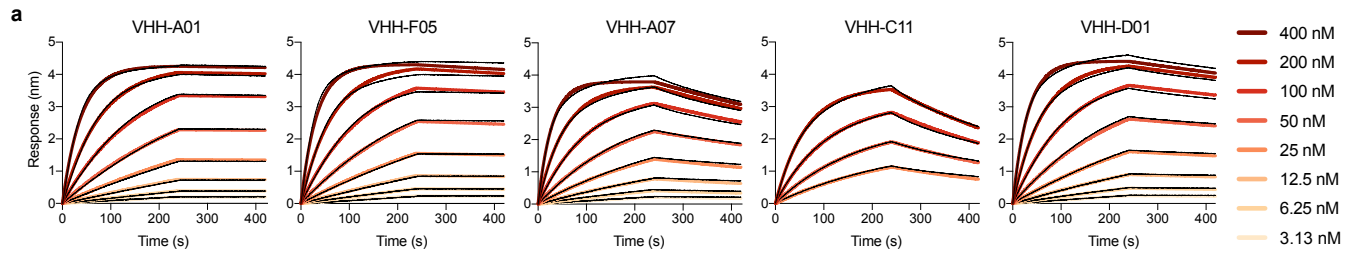
**a****b****c****d****e**

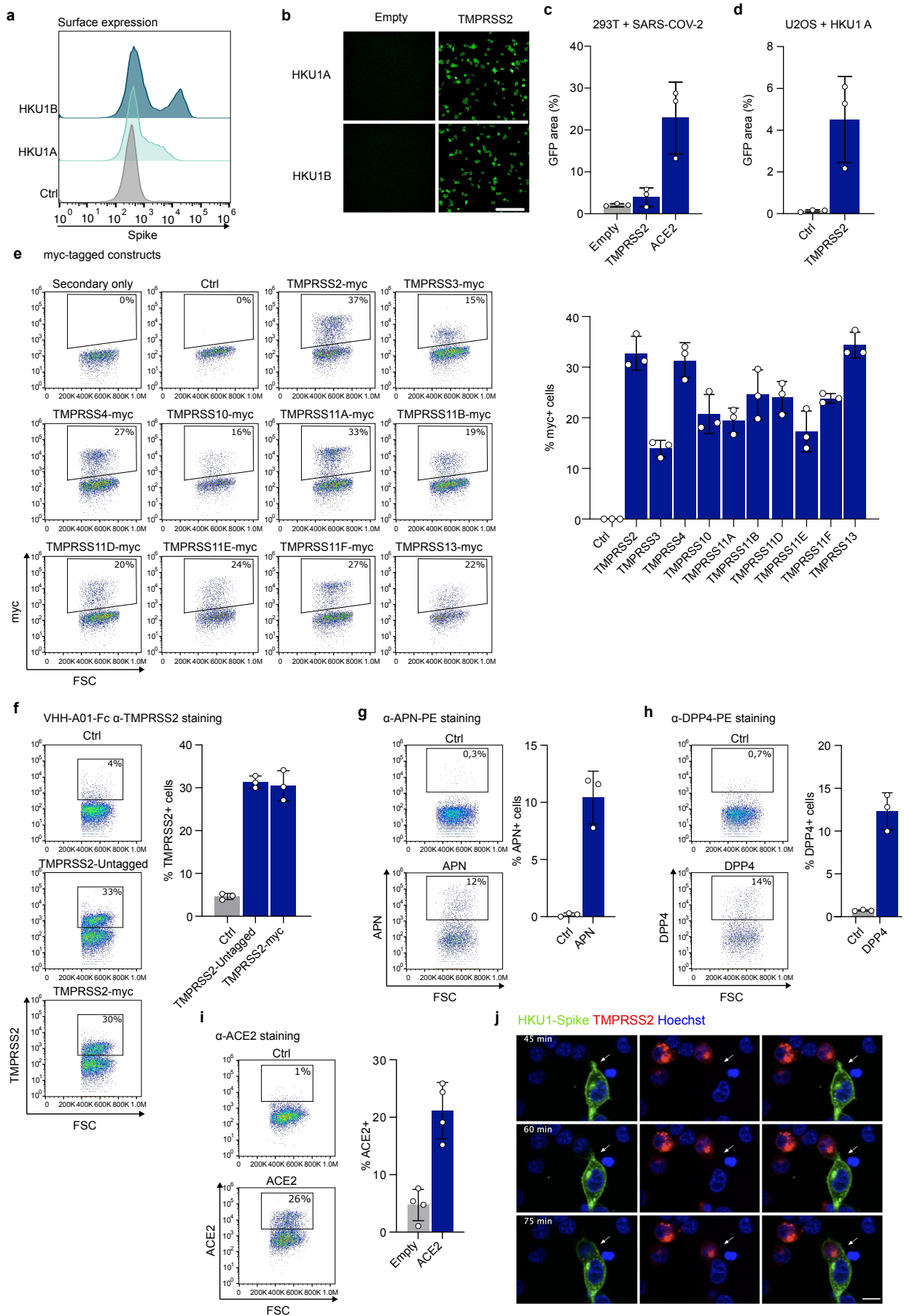


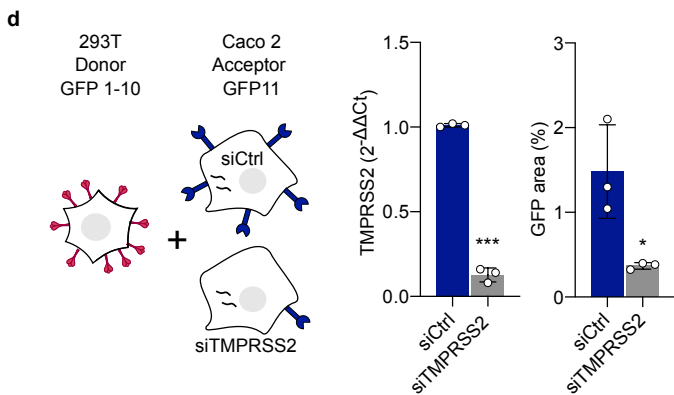
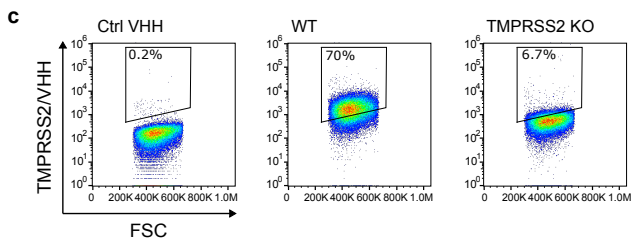
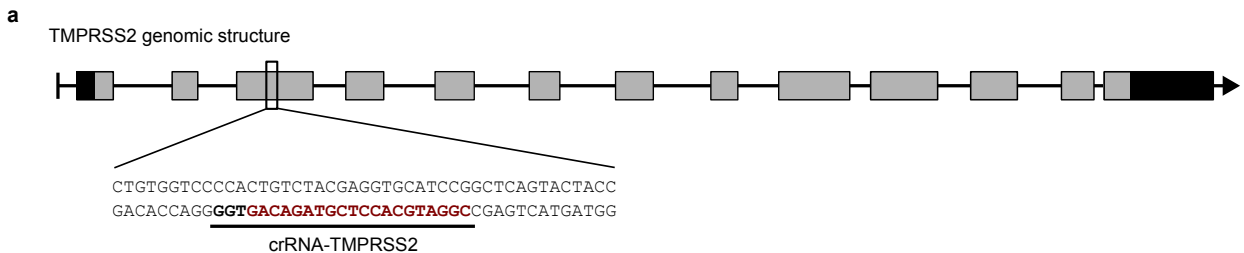




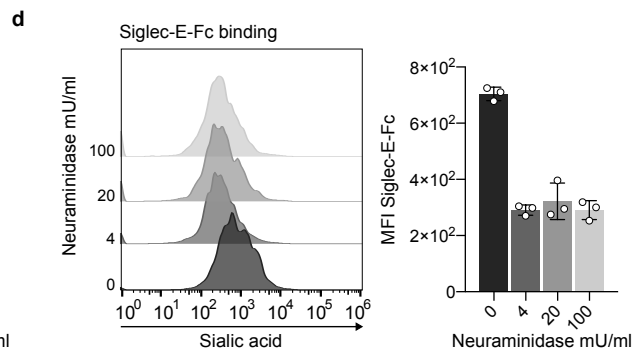
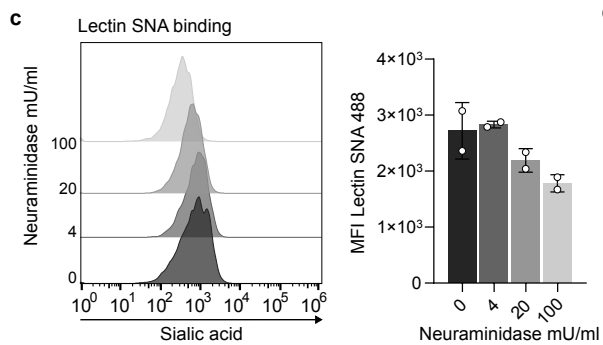
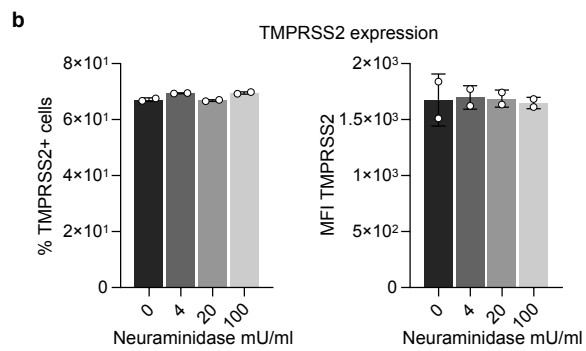
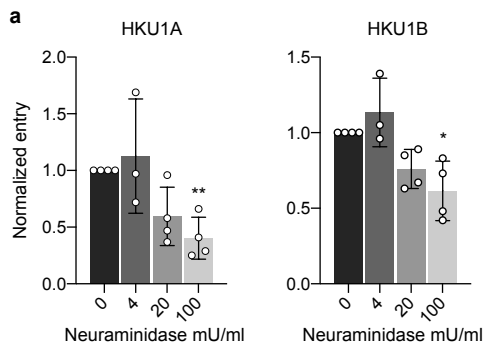
Sensor	Ligand	K <sub>d</sub> (nM)
RBD-HKU1A	TMPRSS2	334.3 ± 66.2
RBD-HKU1B	TMPRSS2	136.7 ± 20.8
RBD-HKU1B-W515A	TMPRSS2	ND
RBD-HKU1B-R517A	TMPRSS2	376.2 ± 96.4
RBD-SARS-CoV-2	TMPRSS2	ND
RBD-HKU1B	ACE2	ND
RBD-SARS-CoV-2	ACE2	92

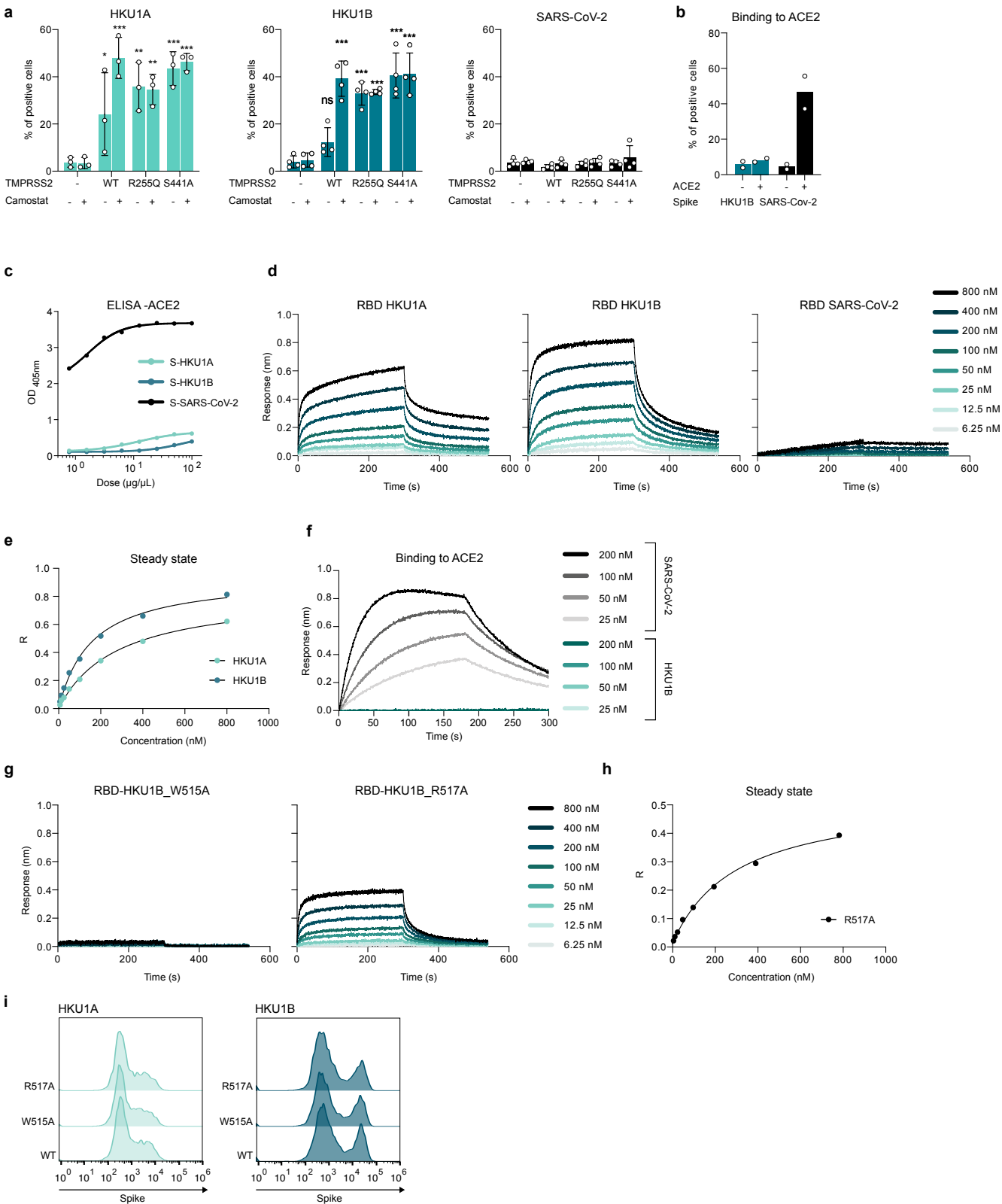


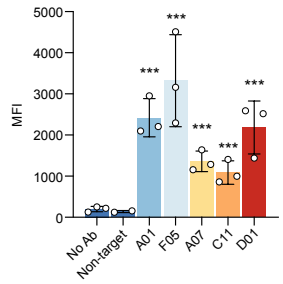
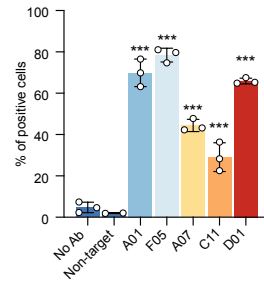
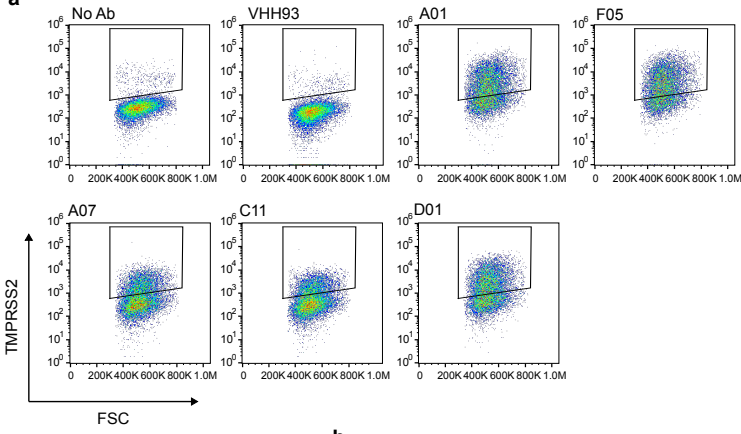
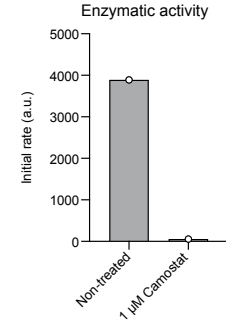
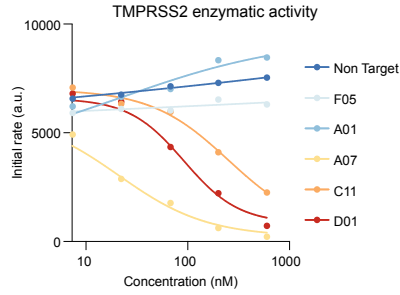
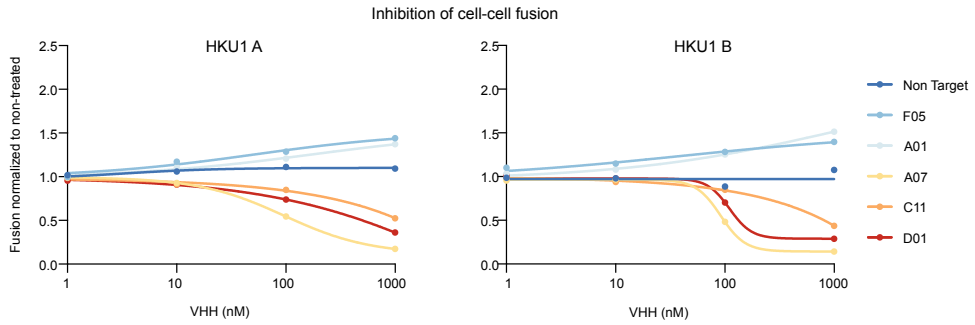
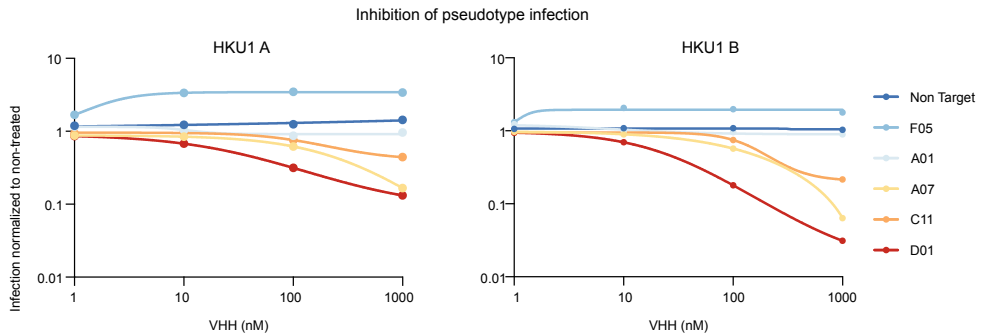










**a****b****c****d**



Nanobody	$k_{on}$ (1/Ms)	$k_{off}$ (1/s)	$K_d$ (nM)	Enzymatic activity inhibition	Cell-cell fusion inhibition	Pseudotype infection inhibition
VHH-A01	$6.4 \cdot 10^4$	$5.1 \cdot 10^{-5}$	0.78	-	-	-
VHH-F05	$7.6 \cdot 10^4$	$1.9 \cdot 10^{-4}$	2.6	-	-	-
VHH-A07	$8.6 \cdot 10^4$	$1.1 \cdot 10^{-3}$	13.3	++	++	++
VHH-C11	$7.0 \cdot 10^4$	$2.3 \cdot 10^{-4}$	32.5	+	+	+
VHH-D01	$7.9 \cdot 10^4$	$4.8 \cdot 10^{-4}$	6.0	+	+	++